

Supporting Information

Tripodal cyanurates as selective transmembrane Cl⁻ transporters

Debashis Mondal,^a Anjana Sathyan,^a Sopan V. Shinde,^a Kamal K. Mishra,^a and Pinaki Talukdar*^a

^aDepartment of Chemistry, Indian Institute of Science Education and Research Pune, Pune 411008, India. E-mail: ptalukdar@iiserpune.ac.in

Table of Contents

Contents	Page Number
1. General Methods	S2
2. Physical Measurements	S2
3. Synthesis of Compounds	S3
4. Anion Binding Study	S9
5. Theoretical Calculations	S14
6. Ion Transport Activity Studies	S24
7. NMR Spectra of Compounds	S38
8. References	S48

1. General Methods

All reagents and compounds used for the synthesis were purchased either from Sigma-Aldrich, Avra chemicals, Spectrochem, Alfa Aesar and used without further purification. Dry solvents MeCN, CH₂Cl₂ and MeOH were purchased from commercially available source, Merck and used without further drying. All the reactions were performed under nitrogen atmospheric environment using N₂ gas balloon and monitored by checking TLC, performed on pre-coated aluminium plates of silica gel 60 F₂₅₄ (0.25 mm, E. Merck). Developed TLC plates were visualized either by ninhydrin staining followed by heating or under a short-wave UV lamp. Column chromatography for purifying the compound was performed using ethyl acetate in hexane or methanol in chloroform as solvents on silica gel (100–200 mesh). HEPES buffer, HPTS dye, Lucigenin dye, Triton X-100, NaOH, and all the inorganic salts (NaCl, NaNO₃, KCl, LiCl, CsCl, NaBr, NaI, etc.) were of molecular biology grade purchased from Sigma Aldrich. Egg yolk phosphatidylcholine (EYPC) lipid (25 mg/mL in chloroform), mini-extruder and polycarbonate membranes (100 and 200 nm) used for the preparation of large unilamellar vesicles (LUVs) were obtained from Avanti Polar Lipids.

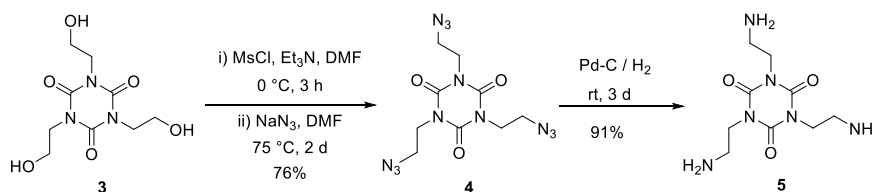
2. Physical Measurements

All ¹H NMR (400 MHz) and ¹³C NMR (100 MHz) spectra were recorded on Bruker 400 MHz and Jeol 400 MHz spectrometers. The chemical shifts (δ) in parts per million were referenced to the residual proton signal of deuterium solvents (¹H NMR CDCl₃: δ 7.26 ppm; ¹³C NMR CDCl₃: δ 77.2 ppm; ¹H NMR CD₃OD: δ 3.31 ppm; ¹³C NMR CD₃OD: δ 49.2 ppm; ¹H NMR DMSO-*d*₆: δ 2.5 ppm; ¹³C NMR DMSO-*d*₆: δ 39.5 ppm). The multiplicities of the peaks are s (singlet), d (doublet), t (triplet), q (quartet), dd (doublet of doublet), ddd (doublet of doublet of doublet), m (multiplet). Coupling constants are reported in Hertz. All the FT-IR spectra were taken and reported in wave numbers (cm⁻¹) using a solution of compound in MeOH/CHCl₃. High resolution mass spectra (HRMS) were acquired in the ESI (+ve) mode. Melting points for all the molecules were recorded in Veego melting point apparatus and the values were uncorrected. The measurement of pH during preparation of buffer solution was done by Helmer pH meter. Fluorescence spectra were recorded on a Fluoromax-4 from JobinYvon Edison equipped with an injector port and a magnetic stirrer and data were processed in Origin 8.5 software. Chloride ion concentration in U-tube experiment was measured using chloride-selective electrode from Accumet.

3. Synthesis of Compounds

3.1. Preparation of trisamine compound 5.

For the preparation of the trisamine molecules we have followed the reported literature procedure.^{S1}

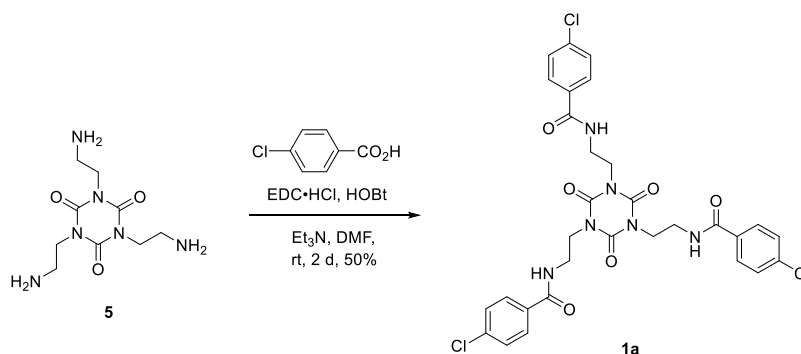


Scheme S1. Preparation of trisamine 5.

3.2. General procedure for amides synthesis

In a 25 mL round bottom flask, trisamine **5** (1.0 equiv.) was taken and dissolved the same in 5 mL of dry DMF. Then substituted benzoic acid (3.2 equiv.), HOBt (3.2 equiv.), EDC.HCl (3.2 equiv.) was added sequentially and reaction mixture was stirred for 5 minutes. Then Et₃N (3.2 equiv.) was added into this and then the whole mixture was allowed to stir under nitrogen atmosphere for 2 days at room temperature. The reaction was monitored in between by checking TLC. After completion of reaction, the DMF was evaporated in high vacuum and the product was extracted into CHCl₃ by the washing with saturated NaHCO₃ solution (10 mL) and water (3 × 10 mL) respectively and followed by brine solution (10 mL). The organic part was then separated from aqueous layer, dried over Na₂SO₄ and the solvent was evaporated in vacuum to get crude product. The crude product was then purified using silica gel column chromatography (2–3% MeOH in CHCl₃) to obtain white solid compound **1a-f** in 31–66% yield.

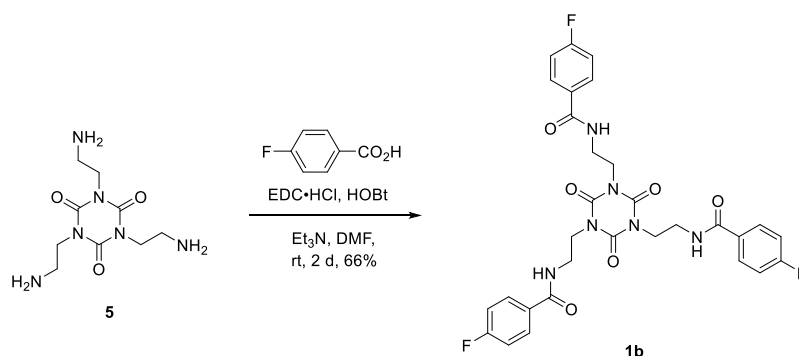
N,N',N''-((2,4,6-trioxo-1,3,5-triazinane-1,3,5-triyl)tris(ethane-2,1-diyl))tris(4-chloro-benzamide) **1a**:



Scheme S2. Synthesis of compound **1a**.

Yield: 50%. **M.p.:** 256 °C; **IR** (neat, v/cm^{-1}): 3856, 3752, 3305, 2103, 1687, 1639, 1546, 1460, 1311, 1181, 1094, 1015, 845, 758, 688; **^1H NMR** (400 MHz, CDCl_3 : $\text{MeOH-}d_4 = 4 : 1$): δ 7.64 (d, $J = 16.9$ Hz, 3H), 7.54 (d, $J = 8.5$ Hz, 6H), 7.25 (d, $J = 8.5$ Hz, 6H), 4.06 – 3.98 (m, 6H), 3.57 – 3.49 (m, 6H); **^{13}C NMR** (101 MHz, CDCl_3 : $\text{MeOH-}d_4 = 4 : 1$): δ 167.8, 149.6, 137.7, 132.3, 128.6, 128.3, 42.5, 37.9; **HRMS (ESI):** Calcd. $\text{C}_{30}\text{H}_{28}\text{Cl}_3\text{N}_6\text{O}_6$ $[\text{M}+\text{H}]^+$: 673.1135, Found: 673.1130, 675.1106.

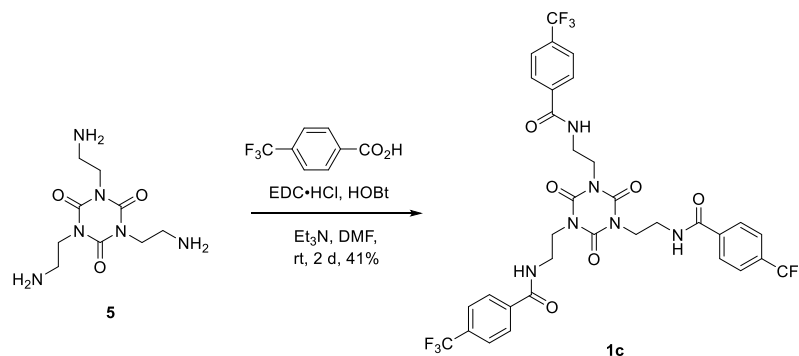
N,N',N'' -((2,4,6-trioxo-1,3,5-triazinane-1,3,5-triyl)tris(ethane-2,1-diyl)tris(4-fluorobenzamide) **1b:**



Scheme S3. Synthesis of compound **1b**.

Yield: 66 %. **M.p.:** > 260 °C; **IR** (neat, v/cm^{-1}): 3960, 3892, 3855, 3818, 3755, 3295, 2312, 2172, 1640, 1502, 1453, 1231, 1113, 1016, 759; **^1H NMR** (400 MHz, $\text{DMSO-}d_6$): δ 8.52 (t, $J = 5.8$ Hz, 3H), 7.81 (dd, $J = 8.4, 5.7$ Hz, 6H), 7.27 (t, $J = 8.8$ Hz, 6H), 3.92 (t, $J = 5.8$ Hz, 6H), 3.44 (dd, $J = 11.5, 5.7$ Hz, 6H).; **^{13}C NMR** (101 MHz, $\text{DMSO-}d_6$): δ 166.1, 165.5, 163.0, 149.6, 131.4, 131.3, 130.2, 130.1, 115.7, 115.5, 42.2, 37.25; **HRMS (ESI):** Calcd. $\text{C}_{30}\text{H}_{28}\text{F}_3\text{N}_6\text{O}_6$ $[\text{M}+\text{H}]^+$: 625.2022, Found: 625.2023.

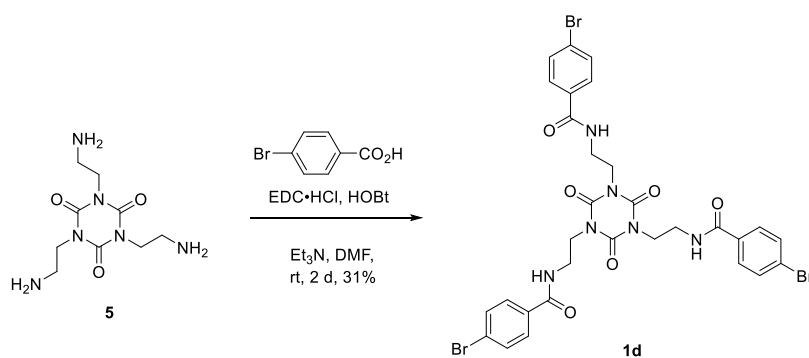
N,N',N'' -((2,4,6-trioxo-1,3,5-triazinane-1,3,5-triyl)tris(ethane-2,1-diyl)tris(4-(trifluoromethyl)benzamide) **1c:**



Scheme S4. Synthesis of compound **1c**.

Yield: 41%. **M.p.:** 183 °C; **IR** (neat, v/cm^{-1}): 3310, 2943, 2834, 1690, 1548, 1456, 1327, 1117, 1019, 754, 661; **^1H NMR** (400 MHz, $\text{DMSO}-d_6$): δ 8.71 (t, $J = 5.8$ Hz, 3H), 7.89 (d, $J = 8.2$ Hz, 6H), 7.79 (d, $J = 8.3$ Hz, 6H), 3.94 (t, $J = 5.8$ Hz, 6H), 3.46 (m, 6H); **^{13}C NMR** (101 MHz, $\text{DMSO}-d_6$): δ 165.9, 149.3, 138.3, 131.41, 131.0, 128.0, 125.6, 125.5, 125.3, 122.6; **HRMS (ESI):** Calcd. $\text{C}_{33}\text{H}_{28}\text{F}_9\text{N}_6\text{O}_6$ $[\text{M}+\text{H}]^+$: 775.1926, Found: 775.1929.

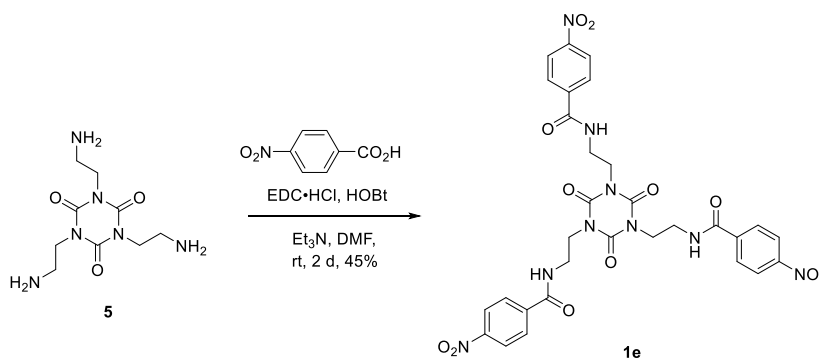
***N,N',N''*-((2,4,6-trioxo-1,3,5-triazinane-1,3,5-triyl)tris(ethane-2,1-diyl))tris(4-bromobenzamide) 1d:**



Scheme S5. Synthesis of compound **1d**.

Yield: 31 %. **M.p.:** 249 °C; **IR** (v/cm^{-1}): 3941, 3884, 3742, 3286, 2927, 2850, 2312, 1686, 1639, 1543, 1456, 1310, 1182, 1106, 1071, 1015, 910, 842, 754, 714, 661; **^1H NMR** (400 MHz, $\text{DMSO}-d_6$): δ 8.59 (t, $J = 5.9$ Hz, 3H), 7.70 – 7.62 (m, 12H), 3.92 (t, $J = 5.9$ Hz, 6H), 3.43 (dd, $J = 11.8, 5.9$ Hz, 6H); **^{13}C NMR** (100 MHz, $\text{DMSO}-d_6$): δ 165.9, 149.2, 133.5, 131.3, 129.2, 124.9, 41.7, 36.8; **HRMS (ESI):** Calcd. $\text{C}_{30}\text{H}_{28}\text{Br}_3\text{N}_6\text{O}_6$ $[\text{M}+\text{H}]^+$: 806.9599, Found: 806.9612.

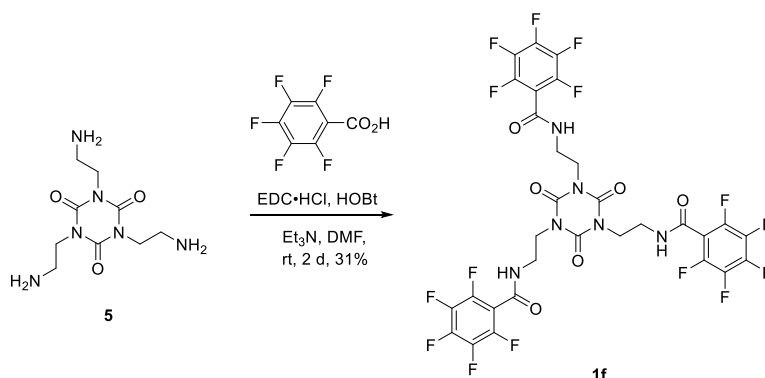
***N,N',N''*-((2,4,6-trioxo-1,3,5-triazinane-1,3,5-triyl)tris(ethane-2,1-diyl))tris(4-nitrobenzamide) 1e:**



Scheme S6. Synthesis of compound **1e**.

Yield: 45%. **M.p.:** 239 °C; **IR** (neat, ν/cm^{-1}): 3268, 2140, 1639, 1459, 1350, 1015, 697, 660; **^1H NMR (400 MHz, DMSO- d_6):** δ 8.82 (t, $J = 5.9$ Hz, 3H), 8.30 (d, $J = 8.9$ Hz, 6H), 7.96 (d, $J = 8.9$ Hz, 6H), 3.96 (t, $J = 5.9$ Hz, 6H), 3.46 (dd, $J = 12.0, 6.1$ Hz, 6H); **^{13}C NMR (101 MHz, DMSO- d_6):** δ 165.2, 149.2, 149.0, 140.1, 128.6, 123.6, 41.6, 37.0; **HRMS (ESI):** Calcd. $\text{C}_{30}\text{H}_{28}\text{N}_9\text{O}_{12}$ $[\text{M}+\text{H}]^+$: 706.1857, Found: 706.1857.

N,N',N'' -((2,4,6-trioxo-1,3,5-triazinane-1,3,5-triyl)tris(ethane-2,1-diyl))tris (2,3,4,5,6-pentafluorobenzamide) **1f:**



Scheme S7. Synthesis of compound **1f**.

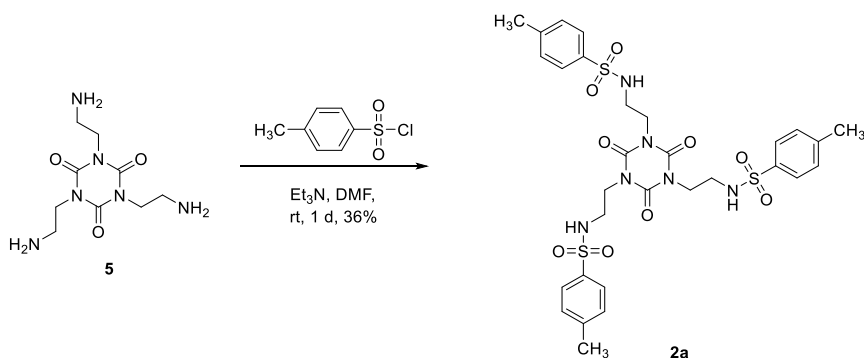
Yield: 31%. **M.p.:** 222 °C; **IR** (neat, ν/cm^{-1}): 3303, 2945, 2833, 1657, 1456, 1114, 1018, 752, 522, 510, 474, 437; **^1H NMR (400 MHz, DMSO- d_6):** δ 9.01 (t, $J = 6.0$ Hz, 3H), 3.96 (t, $J = 6.1$ Hz, 6H), 3.51 (dd, $J = 12.1, 6.0$ Hz, 6H); **HRMS (ESI):** Calcd. $\text{C}_{30}\text{H}_{16}\text{F}_{15}\text{N}_6\text{O}_6$ $[\text{M}+\text{H}]^+$: 841.0892, Found: 841.0883.

3.3. General procedure for sulfonamides synthesis

In a 25 ml round bottom flask, trisamine **5** (1.0 equiv.) was taken and was dissolved in 2 mL of dry DMF. Triethylamine (3.2 equiv.) was added into it under nitrogen atmosphere. In another 10 mL round bottom flask benzenesulphonylchloride (3.2 equiv.) was taken and dissolved in dry DMF under nitrogen atmosphere. Later this solution was added to the previous solution drop wise at 0 °C for 10 minutes. Then the whole reaction mixture was allowed to stir under nitrogen atmosphere for 2 days at RT (reflux at 120 °C for nitro derivative). The reaction was monitored in between by checking TLC. After completion of reaction, the DMF was evaporated in high vacuum and the reaction mixture was washed with saturated NaHCO_3 solution (10 mL) and water (3×10 mL) respectively and followed by brine solution (10 mL). The organic part was then separated from aqueous layer, dried over Na_2SO_4 and the solvent was evaporated in vacuum to get crude product. The crude product

was then purified using silica gel column chromatography (2–3% MeOH in CHCl₃) to obtain white solid compound **2a-e** in 30–47 % yield.

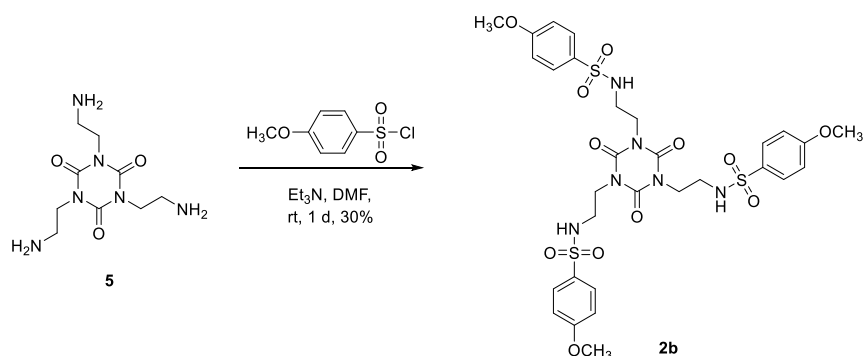
***N,N',N''*-((2,4,6-trioxo-1,3,5-triazinane-1,3,5-triyl)tris(ethane-2,1-diyl)tris(4-methylbenzenesulfonamide) **2a**:**



Scheme S8. Synthesis of compound **2a**.

Yield: 36%. **M.p.:** 84 °C; **IR** (neat, v/cm⁻¹): 3304, 2944, 2834, 1687, 1461, 1324, 1219, 1155, 1097, 1020, 923, 815, 752, 662; **¹H NMR** (400 MHz, CDCl₃): δ 7.70 (d, *J* = 8.3 Hz, 6H), 7.25 (d, *J* = 8.1 Hz, 6H), 5.66 – 5.44 (m, 3H), 4.05 (t, *J* = 5.1 Hz, 6H), 3.29 (dd, *J* = 10.7, 6.0 Hz, 6H), 2.39 (s, 9H); **¹³C NMR** (101 MHz, CDCl₃): δ 149.5, 143.6, 137.3, 129.8, 127.0, 42.8, 40.9, 21.6; **HRMS (ESI):** Calcd. C₃₀H₃₇N₆O₉S₃ [M+H]⁺: 721.1783, Found: 721.1781.

***N,N',N''*-((2,4,6-trioxo-1,3,5-triazinane-1,3,5-triyl)tris(ethane-2,1-diyl)tris(4-methoxybenzenesulfonamide) **2b**:**

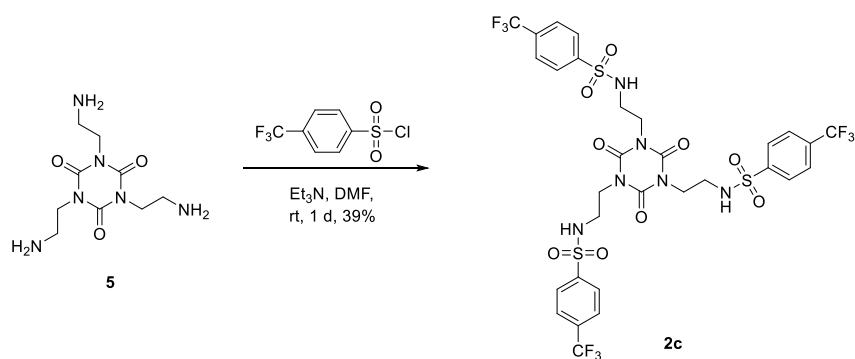


Scheme S9. Synthesis of compound **2b**.

Yield: 30%. **M.p.:** 97 °C; **IR** (neat, v/cm⁻¹): 3332, 2943, 2831, 1453, 1220, 1113, 1022, 750, 663; **¹H NMR** (400 MHz, CDCl₃): δ 7.76 (d, *J* = 8.9 Hz, 6H), 6.92 (d, *J* = 8.9 Hz, 6H), 5.54

(t, $J = 6.4$ Hz, 3H), 4.08 – 3.98 (m, 6H), 3.83 (s, 9H), 3.28 (dd, $J = 10.7, 6.1$ Hz, 6H); ^{13}C NMR (101 MHz, CDCl_3): δ 162.9, 149.5, 131.7, 129.1, 114.3, 55.7, 42.8, 40.8; HRMS (ESI): Calcd. $\text{C}_{30}\text{H}_{37}\text{N}_6\text{O}_{12}\text{S}_3$ $[\text{M}+\text{H}]^+$: 769.1631, Found: 769.1627.

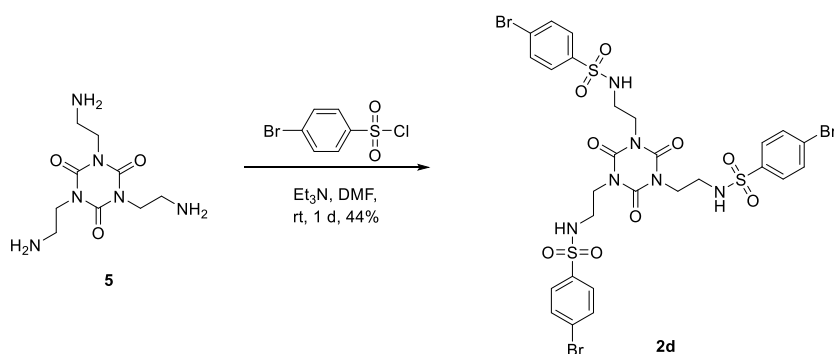
N,N',N''-((2,4,6-trioxo-1,3,5-triazinane-1,3,5-triyl)tris(ethane-2,1-diyl)tris(4-(trifluoromethyl)benzamide) 2c:



Scheme S10. Synthesis of compound 2c.

Yield: 39%. **M.p.:** 125 °C; **IR** (neat, v/cm^{-1}): 3313, 2943, 2832, 1689, 1455, 1326, 1221, 1166, 1111, 1020, 752, 663; ^1H NMR (400 MHz, CDCl_3): δ 7.97 (d, $J = 8.2$ Hz, 6H), 7.75 (d, $J = 8.3$ Hz, 6H), 5.79 (t, $J = 6.0$ Hz, 3H), 4.19 – 4.10 (m, 6H), 3.37 (dd, $J = 10.6, 6.3$ Hz, 6H); ^{13}C NMR (101 MHz, CDCl_3): δ 149.6, 143.6, 134.7, 134.3, 127.4, 126.4, 124.5, 121.8, 42.8, 40.8; HRMS (ESI): Calcd. $\text{C}_{30}\text{H}_{28}\text{F}_9\text{N}_6\text{O}_9\text{S}_3$ $[\text{M}+\text{H}]^+$: 883.0935, Found: 883.0942.

N,N',N''-((2,4,6-trioxo-1,3,5-triazinane-1,3,5-triyl)tris(ethane-2,1-diyl)tris(4-bromobenzenesulfonamide) 2d:

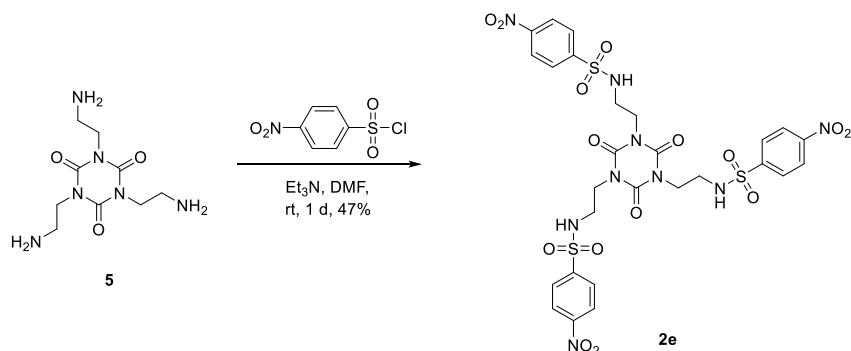


Scheme S11. Synthesis of compound 2d.

Yield: 44%. **M.p.:** 197 °C; **IR** (neat, v/cm^{-1}): 3330, 2943, 2832, 1689, 1458, 1218, 1159, 1108, 1022, 749, 664; ^1H NMR (400 MHz, CDCl_3): δ 7.69 (d, $J = 8.6$ Hz, 6H), 7.62 (d, $J = 8.6$ Hz, 6H), 5.56 (t, $J = 6.1$ Hz, 3H), 4.15 – 4.07 (m, 6H), 3.33 (dd, $J = 10.5, 6.0$ Hz, 6H);

^{13}C NMR (101 MHz, CDCl_3): δ 149.5, 139.2, 132.6, 128.5, 127.9, 42.8, 40.9; HRMS (ESI): Calcd. $\text{C}_{27}\text{H}_{28}\text{Br}_3\text{N}_6\text{O}_9\text{S}_3$ $[\text{M}+\text{H}]^+$: 914.8609, Found: 914.8615, 916.8593.

N,N',N''-((2,4,6-trioxo-1,3,5-triazinane-1,3,5-triyl)tris(ethane-2,1-diyl))tris(4-nitrobenzenesulfonamide) **2e**:^{S2}



Scheme S12. Synthesis of compound **2e**.

Yield: 47% yield. **M.p.:** 125 °C; **IR** (neat, v/cm^{-1}): 3337, 2943, 2831, 1454, 1219, 1112, 1022, 749, 664; **HRMS (ESI):** Calcd. $\text{C}_{27}\text{H}_{28}\text{N}_9\text{O}_{15}\text{S}_3$ $[\text{M}+\text{H}]^+$: 814.0867, Found: 814.0887.

4. Anion Binding Study

4.1. ^1H NMR dilution studies

To check whether any self-association is present in **1c** and in **2c**, we have recorded a series of ^1H NMR spectra by diluting the sample from 3.0 mM to 0.05 mM. In the dilution experiment, we have observed that the N-H proton chemical shift has gradually shifted to downfield region with the broadening of the peaks (Fig. S1 & S2). These results suggested that self-association is present in both the compounds. These results also suggest that carboxyamide **1c** and sulfonamide **2c** are aggregating in different exchange way and we can't predict at what concentration self-association will be stopped.

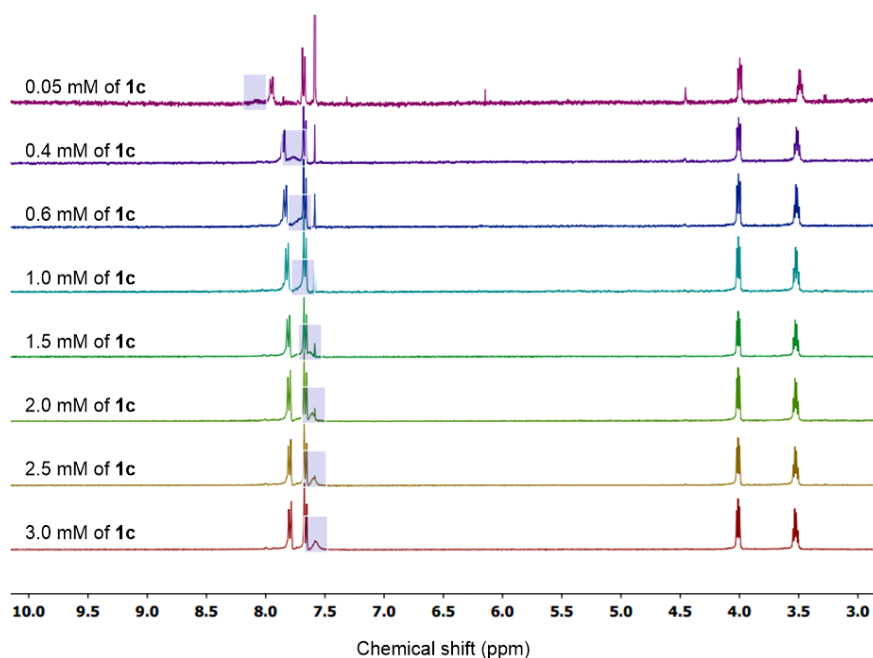


Fig. S1 Stacked plot for ¹H-NMR experiment in Acetonitrile-*d*₃ for compound **1c** with the successive dilution from 3.0 mM to 0.05 mM. The N-H proton chemical shifts are highlighted in blue colour.

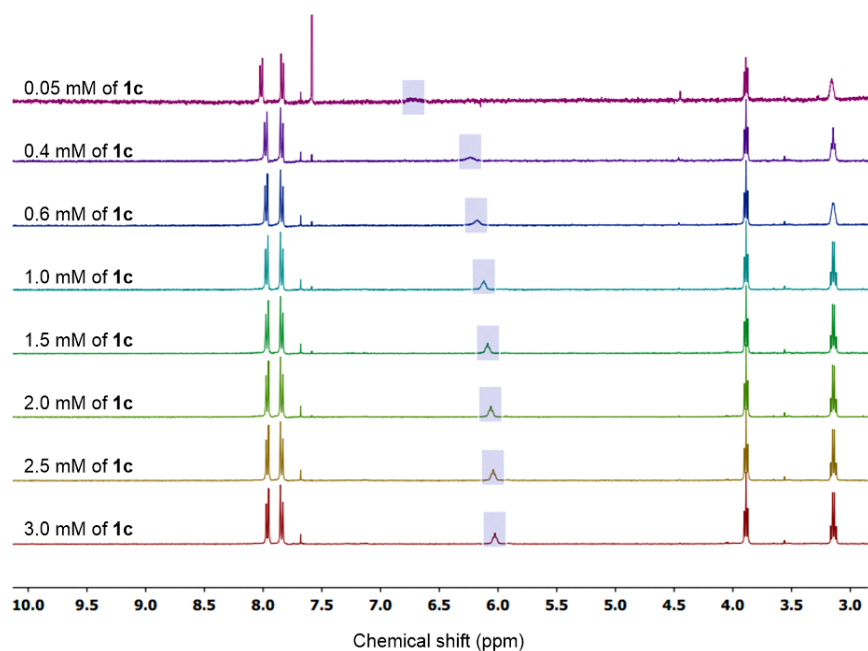


Fig. S2 Stacked plot for ¹H-NMR experiment in Acetonitrile-*d*₃ for compound **2c** with the successive dilution from 3.0 mM to 0.05 mM. The N-H proton chemical shifts are highlighted in blue colour.

4.2. ¹H NMR titration

The proton NMR titration was done in acetonitrile-*d*₃ by successive addition of TBACl. For that, a 300 mM solution of TBACl solution in acetonitrile-*d*₃ was added in a stepwise manner to the stock solution of receptor (3 mM) in acetonitrile-*d*₃. The N-H proton chemical shift of

receptor was monitored and was found to be downfield shifted with the increasing amount of TBACl up to certain limit (Fig. S3 & S4).^{S3}

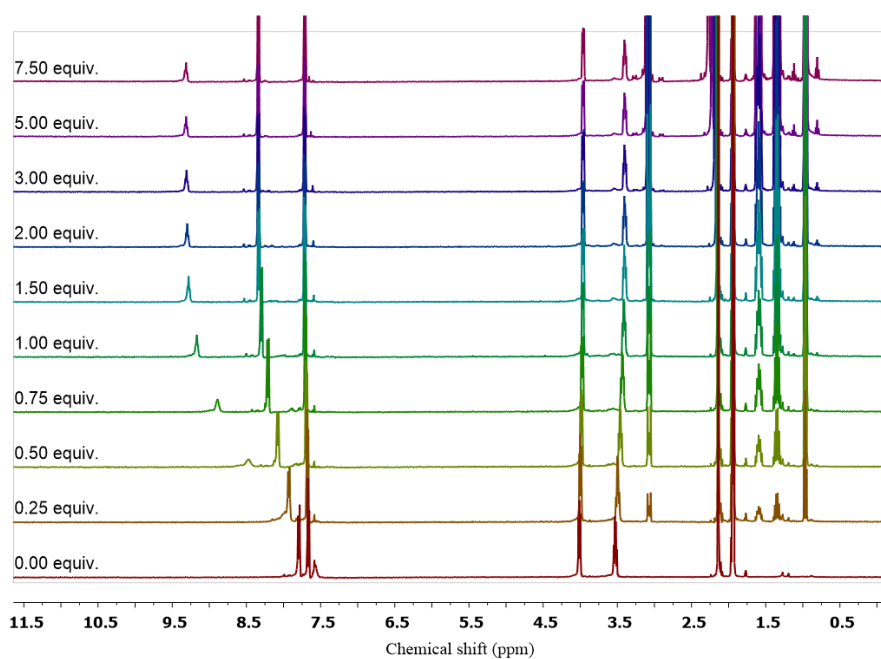


Fig. S3 Stacked plot for ¹H NMR titration experiment in acetonitrile-*d*₃ for compound **1c** with the successive addition of TBACl.

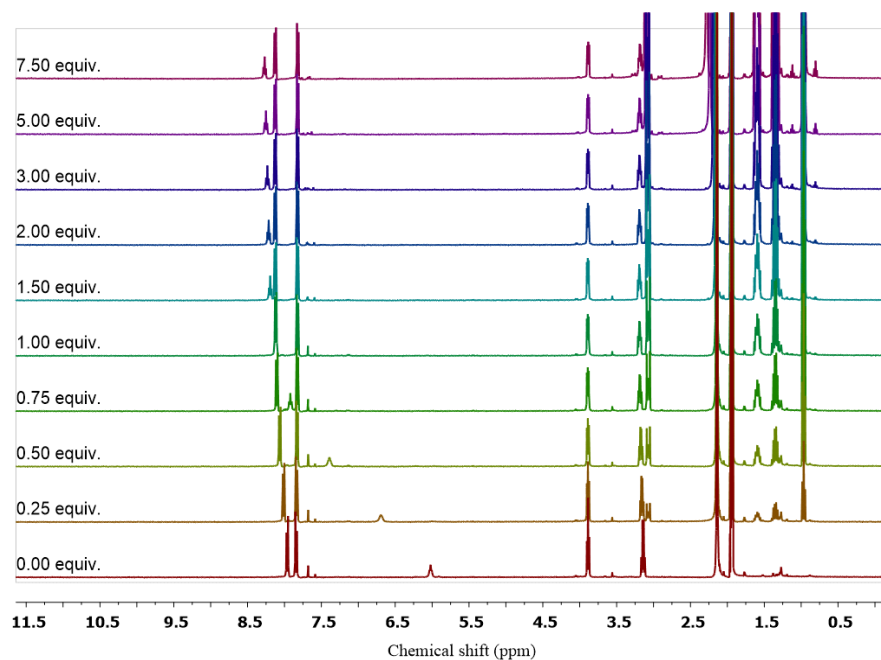


Fig. S4 Stacked plot for ¹H NMR titration experiment in acetonitrile-*d*₃ for compound **2c** with the successive addition of TBACl.

As self-association is there even in the much diluted solution, we have calculated the apparent association constant and the values are $32876 (\pm 23\%) \text{ M}^{-1}$ for carboxyamide **1c** and $21678 (\pm 19\%) \text{ M}^{-1}$ for sulfonamide **2c** (Fig. S5). The apparent dissociation constant values were calculated by fitting the ^1H NMR titration data in a following equation.^{S4}

$$y = P_3 - ((P_3 - P_1) \times (((x + P_4 + P_2) - \sqrt{((x + P_4 + P_2)^2 - (4P_4x))}) / (2P_4))) \quad \text{Eq. S1}$$

where, x is the concentration of TBACl, y is the chemical shift upon addition of TBACl, P_2 is the apparent dissociation constant, P_4 is the concentration of receptor; P_3 and P_1 are the initial and final N-H proton chemical shift, respectively.

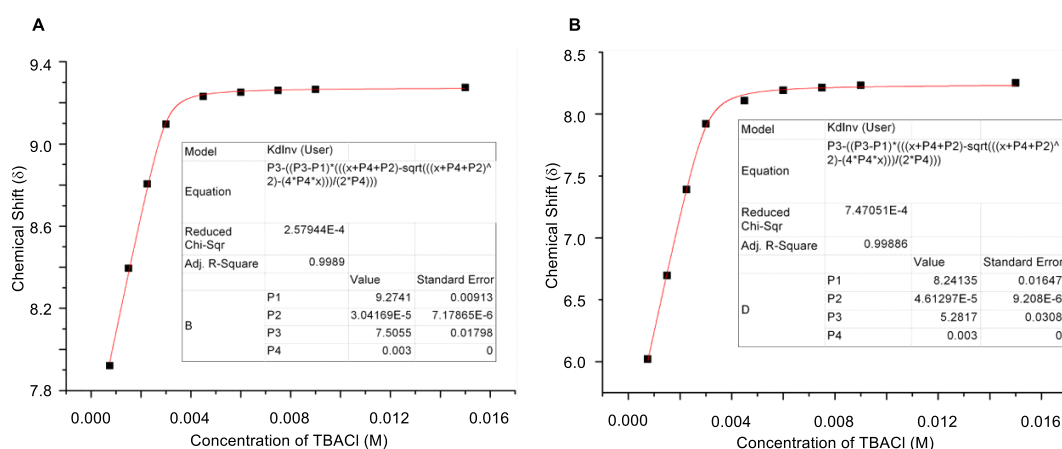


Fig. S5 Fit plot for apparent dissociation constant calculation from ^1H -NMR titration data at 3.0 mM concentration for carboxyamide **1a** (A), and sulfonamide **2c** (B).

4.3. Competitive ^1H NMR titration studies

The ^1H NMR titration experiments for a mixture of two hosts (carboxyamide and sulfonamide) were also carried out at 1 mM concentration of each. For p -CF₃ derivatives (i.e. **1c** and **2c**), the change in the normalized chemical shift (i.e. $\Delta\delta/\Delta\delta_{\text{max}}$) of N-H proton after addition of 1 equivalent of TBACl was slightly less in case of sulfonamide ($\Delta\delta/\Delta\delta_{\text{max}} = 0.57$) compared to that of carboxyamide ($\Delta\delta/\Delta\delta_{\text{max}} = 0.60$) (Fig. S6 and Table 1). Similarly slightly higher $\Delta\delta/\Delta\delta_{\text{max}}$ change was observed for carboxyamide N-H protons compared to sulfonamide N-H protons, when the ^1H NMR titration experiments were done for p -Br and p -NO₂ derivatives (Fig. S7, S8 and Table 1). These results suggest that, for this class of compounds, the change in the normalized chemical shift of sulfonamide N-H proton is always less compared to that of the carboxyamide N-H proton. So the above results indicate

that the described carboxyamide are better receptors for Cl^- compared to corresponding sulfonamide receptors.

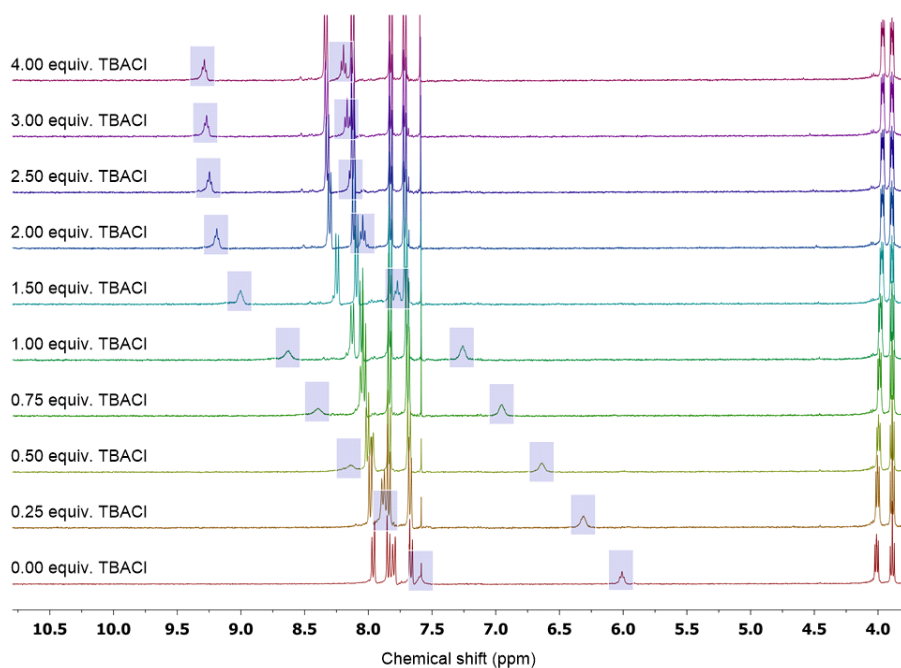


Fig. S6 Stacked plot for ^1H NMR titration experiment in acetonitrile- d_3 for mixture of two hosts (1 equiv. of **1c** and 1 equiv. of **2c**) with the successive addition of TBACl.

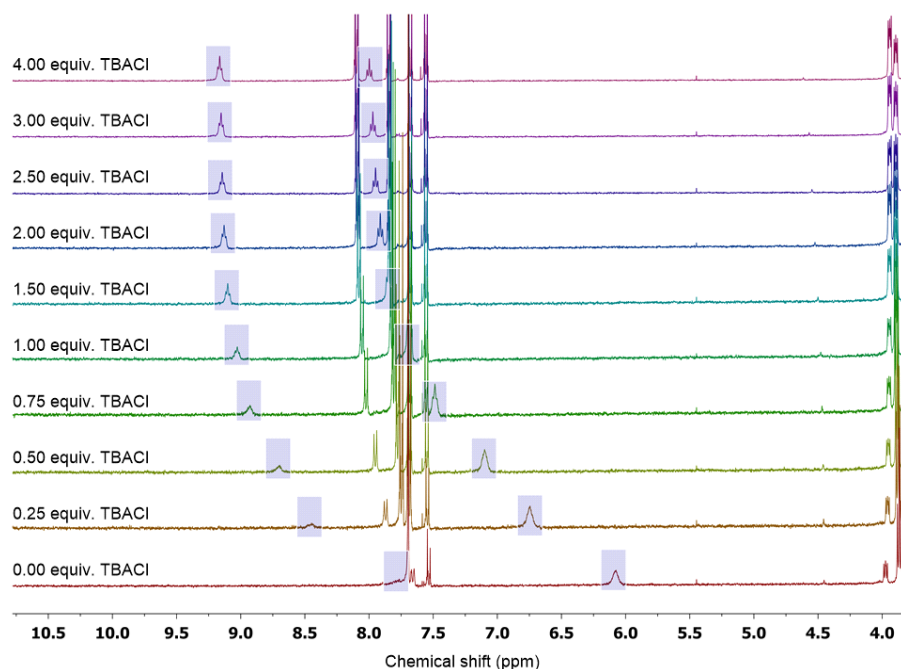


Fig. S7 Stacked plot for ^1H NMR titration experiment in acetonitrile- d_3 for mixture of two hosts (1 equiv. of **1d** and 1 equiv. of **2d**) with the successive addition of TBACl.

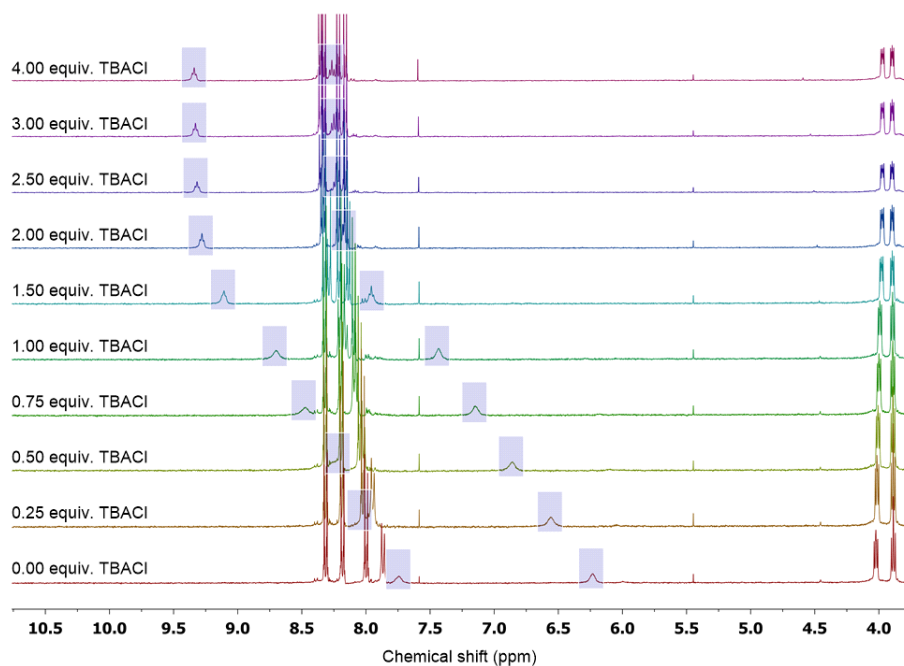


Fig. S8 Stacked plot for ^1H NMR titration experiment in acetonitrile- d_3 for mixture of two hosts (1 equiv. of **1e** and 1 equiv. of **2e**) with the successive addition of TBACl.

Table S1. Normalized chemical shift variation ($\Delta\delta/\Delta\delta_{\text{max}}$) from competitive ^1H NMR titration data.

Derivative	<i>p</i> -Substituent	$\Delta\delta/\Delta\delta_{\text{max}}$ (1 equiv)	$\Delta\delta/\Delta\delta_{\text{max}}$ (2 equiv)
Carboxyamide	-CF ₃	0.60	0.94
	-Br	0.90	0.97
	-NO ₂	0.60	0.96
Sulfonamide	-CF ₃	0.57	0.93
	-Br	0.84	0.95
	-NO ₂	0.59	0.95

5. Theoretical Calculations

5.1. Prediction of conformations

To get an idea about the conformations of **1c**, [**1c**+Cl⁻] complex, **2c**, and [**2c**+Cl⁻] complex, several initial geometries of each systems were generated using the CONFLEX 8^{S5,S6} software package using MMFF94s force field.

For **1c**, the program generated 118 possible conformations. Among these, the top 5 conformations were very similar with Boltzmann populations 45.6886, 15.1626, 13.2945, 6.08141 and 4.79931% (i.e. 85.02642% in total) (Fig. S9B). Therefore, the conformation with the highest Boltzmann population was taken for further geometry optimization.

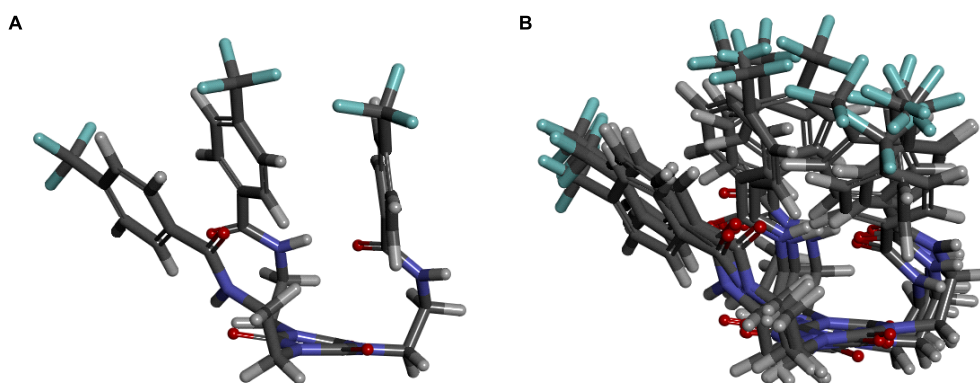


Fig. S9 The conformation of the highest Boltzmann populated geometry of **1c** (A) the overlay image of top 5 Boltzmann populated geometries of **1c** (B).

For [**1c**+Cl⁻] complex, the program generated 135 possible conformations. Among these, the top 23 conformations were very similar with Boltzmann populations 8.90409, 8.77205, 8.64056, 8.50925, 5.30589, 5.27565, 5.23927, 5.20792, 5.17597, 5.14329, 5.10481, 5.07127, 2.57018, 2.55808, 2.54014, 2.52966, 2.48242, 2.47076, 2.45291, 2.44282, 0.910333, 0.903437 and 0.897125% (i.e. 99.10799% in total). (Fig. S10B). Therefore, the conformation with the highest Boltzmann population was taken for further geometry optimization.

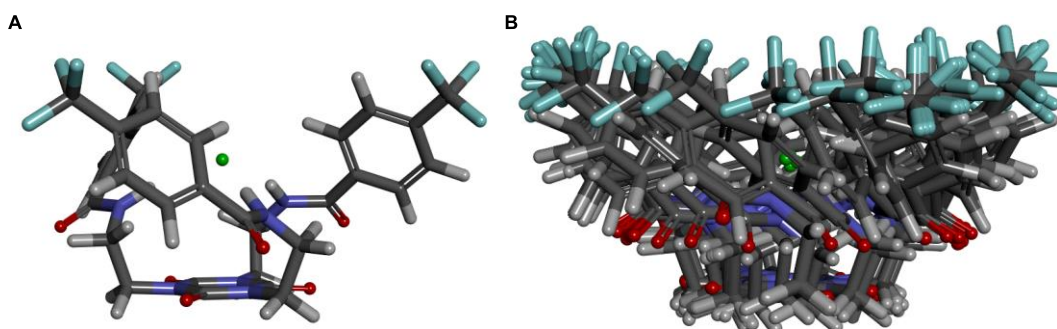


Fig. S10 The conformation of the highest Boltzmann populated geometry of [**1c**+Cl⁻] (A) the overlay image of top 23 Boltzmann populated geometries of [**1c**+Cl⁻] (B).

For **2c**, the program generated 326 possible conformations. Among these, the top 2 conformations were very similar with Boltzmann populations 20.8638 and 19.9479% (i.e. 40.8117% in total) (Fig. S11B). The populations of other conformations were less than 5%. Therefore, the conformation with the highest Boltzmann population was taken for further geometry optimization.

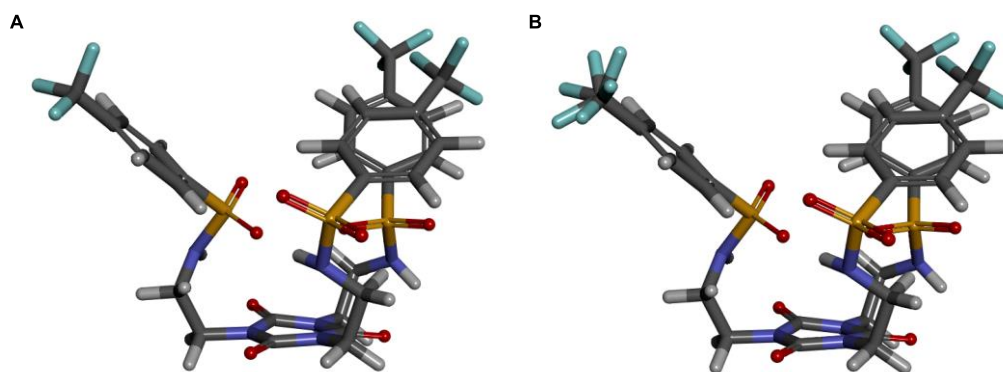


Fig. S11 The conformation of the highest Boltzmann populated geometry of **2c** (A) the overlay image of top 2 Boltzmann populated geometries of **2c** (B).

For $[\mathbf{2c}+\text{Cl}^-]$ complex, the program generated 43 possible conformations. Among these, the Boltzmann population of the most favourable conformation was 88.8617% (Fig. S12B). Therefore, this conformation was taken for further geometry optimization.

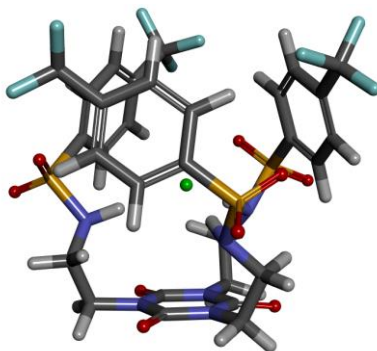


Fig. S12 The conformation of the highest Boltzmann populated geometry of $[\mathbf{2c}+\text{Cl}^-]$.

5.2. Geometry optimization and binding energy calculation

The geometry optimization for each system was carried out by Gaussian 09 program package^{S7} using B3LYP functional and 6-31G basis set.^{S8}

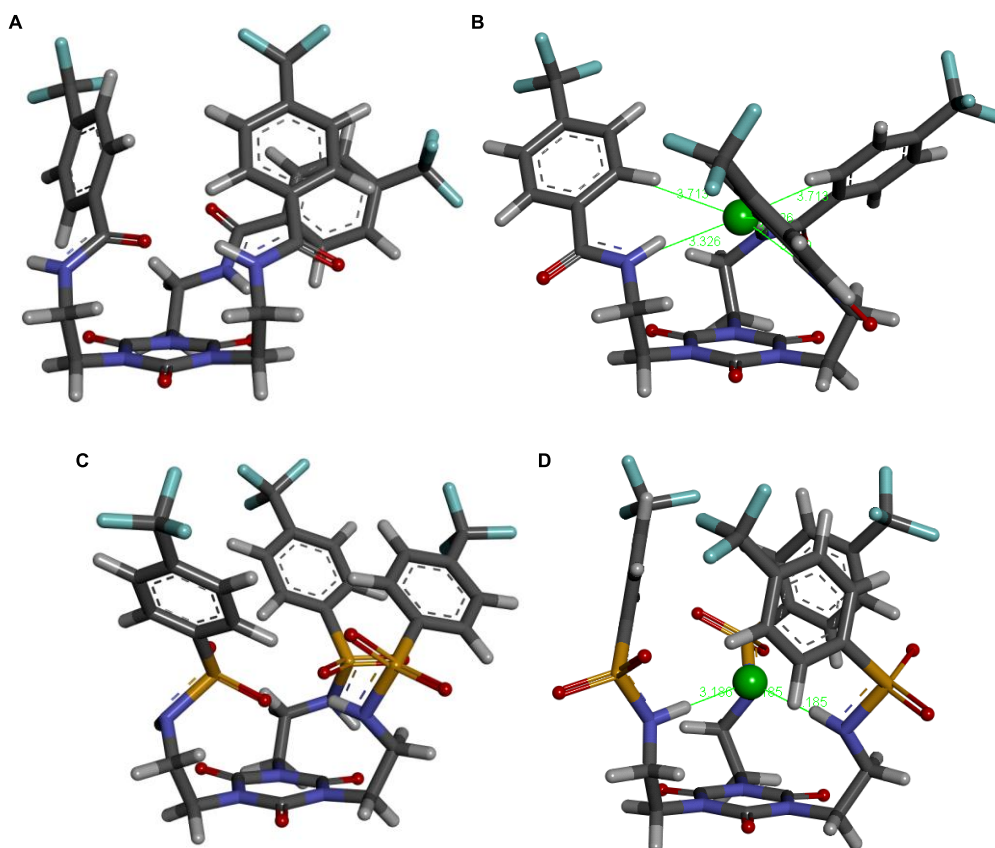


Fig. S13 The geometry optimized structures of **1c** (A), **[1c+Cl⁻]** complex (B), **2c** (C), and **[2c+Cl⁻]** complex (D).

The zero point energy (ZPE) and basis set superposition error (BSSE)^{S7, S9} corrected binding energy (BE) calculation for **[1c+Cl⁻]** and **[2c+Cl⁻]** was performed by Gaussian 09 program package at the same level. The binding energy (*BE*) was calculated using the following relation:

$$BE = [HF_{[L+Cl^-]} + ZPE_{[L+Cl^-]} + BSSE_{[L+Cl^-]}] - [HF_L + ZPE_L] - [HF_{Cl^-}] \quad \text{Eq. S2}$$

where, $HF_{[L+Cl^-]}$ = electronic energy of **[L+Cl⁻]** complex, $ZPE_{[L+Cl^-]}$ = ZPE of **[L+Cl⁻]** complex, $BSSE_{[L+Cl^-]}$ = BSSE of **[L+Cl⁻]** complex, HF_L = electronic energy of ligand **L**, ZPE_L = ZPE of ligand **L**, HF_{Cl^-} = electronic energy of ligand **Cl⁻**, and **L** = ligand (i.e. either **1c** or **2c**).

Table S2. Atomic coordinates of the optimized structure of lowest energy conformation obtained for **1c** from DFT B3LYP/6-31G geometry optimization.

Charge = 0		Multiplicity = 1			
Atom #	Atom Type	x	y	z	
1	C	3.956283	-3.192636	-0.465851	
2	C	4.060813	-1.634097	1.447556	
3	N	4.607031	-2.224772	0.308662	
4	N	2.812928	-2.130361	1.837923	
5	N	2.654586	-3.509353	-0.082149	
6	O	4.505291	-3.710946	-1.452625	
7	O	4.650146	-0.740813	2.085904	
8	C	1.292373	-0.485538	3.04867	
9	H	1.17768	-0.038671	4.043269	
10	H	1.714238	0.300087	2.407471	
11	C	5.721641	-0.777193	-1.378106	
12	H	6.704728	-0.489187	-1.765796	
13	H	5.17223	-1.276152	-2.178472	
14	C	1.856743	-4.353899	-1.014155	
15	H	0.924502	-4.588367	-0.503701	
16	H	2.418352	-5.271623	-1.20439	
17	C	5.911044	-1.741224	-0.193877	
18	H	6.488449	-2.608865	-0.518006	
19	H	6.411555	-1.253804	0.642669	
20	C	2.263689	-1.664927	3.145062	
21	H	3.128451	-1.366992	3.737252	
22	H	1.780884	-2.525028	3.614095	
23	C	1.572041	-3.627023	-2.340876	
24	H	2.506798	-3.405156	-2.857406	
25	H	0.976974	-4.306092	-2.959512	
26	C	2.883326	3.633088	0.934414	
27	C	3.094179	1.917636	-0.770746	
28	C	2.222764	2.639839	-1.602315	
29	C	1.704797	3.864057	-1.179587	
30	H	-4.516453	-0.058956	-2.069612	
31	C	-3.619547	2.4651	-1.627606	
32	C	-2.802559	1.228989	-1.789336	
33	C	-3.437932	-0.003917	-1.989998	
34	C	1.444769	5.650342	0.555902	
35	H	1.056547	4.438098	-1.831398	
36	H	1.970505	2.244694	-2.579723	
37	H	-1.941038	-2.674323	2.092844	
38	H	-4.138752	-3.338115	1.216197	
39	O	2.952506	-0.22922	-1.874175	
40	H	-3.142314	-2.131532	-2.213484	
41	H	-5.428445	0.770957	1.280605	
42	C	-2.686726	-1.907759	1.912903	
43	C	-2.416124	-0.553154	2.173779	
44	C	-3.93362	-2.294147	1.420532	
45	C	-3.420807	0.403861	1.960454	
46	C	-4.920854	-1.327024	1.191806	
47	C	-4.666358	0.023787	1.464708	
48	N	0.829553	-2.380601	-2.169433	

49	H	1.355209	-1.514072	-2.200304
50	C	-1.273918	-1.112192	-1.959442
51	O	-1.155689	-3.507742	-2.054446
52	C	-0.533964	-2.41287	-2.058083
53	C	-6.205976	-1.720948	0.551042
54	H	-3.198863	1.44236	2.171718
55	N	-0.025632	-0.89969	2.570435
56	H	-0.092759	-1.804475	2.119446
57	C	2.0417	4.362367	0.08688
58	H	3.122747	4.01618	1.91885
59	C	3.416832	2.416152	0.503661
60	C	-1.409906	1.292764	-1.658747
61	H	-0.927091	2.246849	-1.486227
62	O	0.903399	-3.359848	1.423433
63	H	4.046638	1.837782	1.173373
64	C	2.052556	-3.022532	1.073372
65	O	-0.964222	1.102586	3.149005
66	C	-1.092191	-0.054258	2.671802
67	H	0.428844	0.198716	-1.638685
68	C	-0.647435	0.127323	-1.748313
69	C	-2.67334	-1.165902	-2.070831
70	N	4.983588	0.431098	-1.008926
71	H	5.48601	1.166986	-0.533157
72	C	3.656703	0.620064	-1.259266
73	F	0.193429	5.474411	1.139678
74	F	1.267143	6.550179	-0.492546
75	F	2.242855	6.277914	1.508362
76	F	-6.139977	-1.639836	-0.852278
77	F	-7.267173	-0.904467	0.927575
78	F	-6.570706	-3.033071	0.83642
79	F	-4.056931	2.652529	-0.307656
80	F	-4.770729	2.448049	-2.409313
81	F	-2.91096	3.61735	-1.961657

Table S3. Atomic coordinates of the optimized structure of lowest energy conformation obtained for [**1c**+Cl⁻] from DFT B3LYP/6-31G geometry optimization.

Charge = -1		Multiplicity = 1			
Atom #	Atom Type	x	y	z	
1	Cl	0.012437	-0.007344	-0.059662	
2	C	-0.992911	1.026782	3.54255	
3	C	-0.338296	-1.353905	3.558077	
4	N	-1.295979	-0.337288	3.555575	
5	N	0.994518	-0.933878	3.551968	
6	N	0.366179	1.348146	3.537867	
7	O	-1.887351	1.892405	3.555918	
8	O	-0.640509	-2.561054	3.586295	
9	C	2.171751	-2.596145	2.084583	
10	H	2.878931	-3.428568	2.145173	
11	H	1.204542	-2.975829	1.748449	
12	C	-3.315534	-0.543375	2.079208	

13	H	-4.391612	-0.7317	2.136252
14	H	-3.151576	0.478478	1.730202
15	C	0.758976	2.776473	3.45283
16	H	1.588217	2.930594	4.146454
17	H	-0.104328	3.363758	3.762195
18	C	-2.730383	-0.711974	3.492707
19	H	-3.268665	-0.067948	4.191365
20	H	-2.802844	-1.751874	3.807772
21	C	2.03632	-1.988502	3.491988
22	H	1.755397	-2.768742	4.202595
23	H	2.975592	-1.526353	3.792176
24	C	1.191931	3.179029	2.031851
25	H	1.563155	4.207255	2.073057
26	H	1.995802	2.524713	1.687531
27	C	-1.018954	-4.206468	-1.787827
28	C	-2.609154	-3.642007	-0.041969
29	C	-3.160593	-4.930199	-0.147335
30	C	-2.65474	-5.848966	-1.062993
31	H	-4.40051	6.071181	-1.195203
32	C	-5.08395	4.097381	-2.914257
33	C	-3.995921	4.070932	-1.899834
34	C	-3.755593	5.204192	-1.109144
35	C	-1.079378	-6.439207	-2.913946
36	H	-3.080061	-6.84333	-1.134493
37	H	-3.987403	-5.18055	0.50624
38	H	6.499875	-0.833986	0.47877
39	H	7.464622	0.782228	-1.175106
40	O	-4.216009	-3.12544	1.664009
41	H	-2.489175	6.057503	0.424386
42	H	3.478896	1.774747	-2.4655
43	C	5.861881	-0.256771	-0.179367
44	C	4.472708	-0.43932	-0.071281
45	C	6.392535	0.639846	-1.102573
46	C	3.615292	0.299419	-0.904481
47	C	5.530894	1.374518	-1.930322
48	C	4.144701	1.20095	-1.831561
49	N	0.100133	3.124947	1.063244
50	H	-0.029157	2.243811	0.567286
51	C	-1.861799	4.077512	-0.080295
52	O	-0.59888	5.239125	1.597218
53	C	-0.744547	4.181915	0.922142
54	C	6.098085	2.282749	-2.963257
55	H	2.536412	0.194582	-0.845361
56	N	2.669648	-1.643999	1.095089
57	H	1.970862	-1.099393	0.590708
58	C	-1.577641	-5.487149	-1.884946
59	H	-0.181349	-3.930733	-2.417806
60	C	-1.529834	-3.28631	-0.868979
61	C	-3.170396	2.945616	-1.783954
62	H	-3.361871	2.06779	-2.389764
63	O	2.592834	0.745711	3.551039
64	H	-1.068893	-2.305275	-0.811545
65	C	1.396045	0.403685	3.539676
66	O	4.850821	-2.071225	1.64715

67	C	4.006792	-1.437516	0.953728
68	H	-1.491567	2.055281	-0.803862
69	C	-2.107937	2.945881	-0.876314
70	C	-2.696873	5.20088	-0.205292
71	N	-2.739786	-1.466523	1.104707
72	H	-1.915444	-1.143049	0.599751
73	C	-3.238489	-2.72527	0.97204
74	F	0.272234	-6.261249	-3.204899
75	F	-1.750656	-6.314719	-4.138396
76	F	-1.239697	-7.773236	-2.533585
77	F	5.241398	3.332158	-3.290279
78	F	6.373883	1.626556	-4.171192
79	F	7.30801	2.856363	-2.565627
80	F	-4.671244	4.640964	-4.138879
81	F	-6.173233	4.873086	-2.510852
82	F	-5.578412	2.828545	-3.210553

Table S4. Atomic coordinates of the optimized structure of lowest energy conformation obtained for **2c** from DFT B3LYP/6-31G geometry optimization.

Charge = 0		Multiplicity = 1		
Atom #	Atom Type	x	y	z
1	C	-0.635294	-4.247506	-0.515321
2	C	-2.9787	-3.684561	-0.011762
3	N	-1.684555	-4.060838	0.374893
4	N	-3.131701	-3.375201	-1.372952
5	N	-0.883546	-3.896996	-1.847287
6	O	0.467202	-4.710445	-0.160572
7	O	-3.93868	-3.653338	0.768957
8	C	-4.7668	-1.46175	-1.648014
9	H	-5.776314	-1.257532	-2.023828
10	H	-4.759037	-1.221493	-0.580865
11	C	-0.486556	-3.220552	2.431294
12	H	-0.408014	-3.439029	3.501725
13	H	0.510935	-3.277724	1.980687
14	C	0.208814	-4.058534	-2.833504
15	H	-0.271311	-4.124487	-3.810666
16	H	0.706635	-5.006632	-2.616373
17	C	-1.416919	-4.281691	1.823015
18	H	-0.959501	-5.26797	1.934856
19	H	-2.387985	-4.257944	2.314405
20	C	-4.473271	-2.960026	-1.836839
21	H	-5.202884	-3.53269	-1.261433
22	H	-4.542513	-3.236734	-2.889942
23	C	1.225996	-2.906297	-2.869329
24	H	1.786922	-2.981966	-3.808691
25	H	0.690502	-1.951258	-2.885968
26	C	3.468618	-0.464626	3.746724
27	C	1.150481	-0.120873	3.274096
28	C	1.4211	0.947773	2.426505
29	C	2.755165	1.314608	2.239094
30	H	1.794083	2.530354	-3.205797

31	C	4.402774	3.219736	-3.406989
32	C	3.829329	2.06465	-2.650475
33	C	2.446656	1.838684	-2.687044
34	C	5.194952	0.962118	2.624148
35	H	3.004108	2.155071	1.602253
36	H	0.610839	1.484807	1.949765
37	H	-2.722152	1.156915	1.399005
38	H	-3.656447	3.263201	2.329067
39	O	-1.5424	0.67254	3.118519
40	H	0.827489	0.555485	-2.023695
41	H	-4.76034	4.565117	-1.633044
42	C	-3.169158	1.898878	0.740903
43	C	-3.243516	1.718637	-0.635769
44	C	-3.690228	3.090936	1.260241
45	C	-3.794183	2.642946	-1.519259
46	C	-4.257984	4.040359	0.401997
47	C	-4.310468	3.824315	-0.9837
48	N	2.223478	-2.923812	-1.770801
49	H	2.253759	-3.797531	-1.234298
50	C	2.784636	-0.124208	-1.378316
51	O	0.52029	-1.2792	-0.150135
52	S	2.089683	-1.621449	-0.502111
53	C	-4.753556	5.335877	0.961922
54	H	-3.834044	2.446143	-2.583425
55	N	-3.844613	-0.545242	-2.35883
56	H	-3.375122	-0.942782	-3.181126
57	C	3.771485	0.60282	2.893304
58	H	4.26281	-0.997135	4.254656
59	C	2.134693	-0.831483	3.94938
60	C	4.686313	1.194024	-1.961971
61	H	5.749256	1.396224	-1.918062
62	O	-2.24614	-2.958066	-3.465601
63	H	1.866097	-1.630868	4.629315
64	C	-2.092673	-3.370292	-2.295351
65	O	-2.243996	-0.82398	-0.04547
66	S	-2.503529	0.150396	-1.33475
67	H	4.788926	-0.595928	-0.741138
68	C	4.158964	0.076048	-1.310111
69	C	1.90113	0.728623	-2.032207
70	N	-1.098641	-1.893744	2.287427
71	H	-1.099406	-1.466739	1.352331
72	S	-0.648897	-0.648703	3.496785
73	F	6.050347	0.555684	3.640151
74	F	5.367722	2.334625	2.458765
75	F	5.682113	0.376131	1.447089
76	F	-5.26177	5.192025	2.247113
77	F	-5.758171	5.894552	0.176559
78	F	-3.739889	6.291173	1.041487
79	F	4.681844	2.887821	-4.733885
80	F	5.596817	3.670558	-2.8553
81	F	3.529419	4.302406	-3.450833
82	O	-0.726755	-1.377473	4.958858
83	O	-1.305589	0.475123	-2.410978
84	O	3.100686	-2.087227	0.69693

Table S5. Atomic coordinates of the optimized structure of lowest energy conformation obtained for [2c+Cl⁻] from DFT B3LYP/6-31G geometry optimization.

Charge = -1		Multiplicity = 1			
Atom #	Atom Type	x	y	z	
1	Cl	1.009067	-0.001392	0.002036	
2	C	4.398229	1.373022	0.395841	
3	C	4.401415	-1.01821	1.010974	
4	N	4.378651	0.34282	1.337471	
5	N	4.386935	-1.318646	-0.351995	
6	N	4.385896	0.975233	-0.946173	
7	O	4.459356	2.567505	0.739211	
8	O	4.466282	-1.912292	1.873934	
9	C	3.101639	-3.500322	-0.349314	
10	H	3.192885	-4.52246	-0.733739	
11	H	3.008495	-3.541787	0.740485	
12	C	3.084894	1.435366	3.220484	
13	H	3.171305	1.613162	4.298331	
14	H	2.9933	2.400013	2.711488	
15	C	4.380509	2.032571	-1.98997	
16	H	5.240053	1.863703	-2.645615	
17	H	4.495184	2.975528	-1.458235	
18	C	4.364622	0.71767	2.775093	
19	H	5.217717	1.377354	2.959985	
20	H	4.485418	-0.213455	3.325994	
21	C	4.379212	-2.751072	-0.746352	
22	H	5.233459	-3.237828	-0.2663	
23	H	4.501522	-2.76194	-1.82803	
24	C	3.10843	2.057495	-2.845749	
25	H	3.199972	2.901925	-3.538154	
26	H	3.02319	1.133969	-3.426944	
27	C	-2.957714	-0.933306	3.031814	
28	C	-0.688092	-0.3573	3.501991	
29	C	-0.23523	-1.63358	3.185872	
30	C	-1.175077	-2.580935	2.762919	
31	H	-0.821429	3.909139	1.851436	
32	C	-3.517274	3.58646	1.656916	
33	C	-2.507461	3.481384	0.564177	
34	C	-1.149323	3.692308	0.84206	
35	C	-3.541453	-3.225906	2.247512	
36	H	-0.847933	-3.564306	2.447639	
37	H	0.819625	-1.872834	3.226591	
38	H	0.847033	-1.860891	-3.22401	
39	H	-0.817809	-0.34319	-4.307769	
40	O	1.045142	0.764182	5.60285	
41	H	0.846344	3.723041	-0.001835	
42	H	-3.984569	-2.252124	-2.081013	
43	C	-0.20897	-1.948119	-3.002988	
44	C	-0.665348	-2.861786	-2.05914	
45	C	-1.147084	-1.109787	-3.616897	
46	C	-2.002206	-2.992319	-1.700901	

47	C	-2.505348	-1.24263	-3.294911
48	C	-2.934958	-2.171475	-2.335903
49	N	1.928595	2.302843	-1.995968
50	H	1.597067	1.501457	-1.421482
51	C	-0.664529	3.21441	-1.452398
52	O	1.080166	4.455303	-3.476117
53	S	0.536431	3.025424	-2.878306
54	C	-3.513319	-0.345234	-3.930153
55	H	-2.295675	-3.687796	-0.926096
56	N	1.927927	-2.883625	-0.995074
57	H	1.595905	-1.98516	-0.589199
58	C	-2.531762	-2.230261	2.710178
59	H	-4.006002	-0.668137	2.969127
60	C	-2.022989	0.023599	3.429012
61	C	-2.935415	3.113525	-0.719762
62	H	-3.985043	2.934651	-0.918355
63	O	4.480696	-0.655393	-2.572719
64	H	-2.313242	1.043684	3.64197
65	C	4.408966	-0.355302	-1.367267
66	O	1.074544	-5.23791	-2.125333
67	S	0.533194	-4.005845	-1.183943
68	H	-2.293336	2.646377	-2.736092
69	C	-2.001192	2.970899	-1.746383
70	C	-0.209638	3.576628	-0.189127
71	N	1.912434	0.567371	3.003679
72	H	1.586357	0.470488	2.020631
73	S	0.512541	0.967573	4.06262
74	F	-3.803441	-3.14314	0.869927
75	F	-4.781071	-3.041628	2.86583
76	F	-3.159166	-4.53762	2.489287
77	F	-3.121575	0.110731	-5.180509
78	F	-3.788177	0.800129	-3.164675
79	F	-4.748456	-0.977999	-4.095336
80	F	-4.751345	4.045039	1.187998
81	F	-3.126731	4.443962	2.675213
82	F	-3.794019	2.352922	2.269231
83	O	-0.213439	2.413691	3.744334
84	O	-0.199264	-4.453196	0.224202
85	O	-0.195609	2.028908	-3.969538

6. Ion transport activity studies

6.1. Determination of Ion transport activity by HPTS assay

6.1.1. Preparation of buffer, HPTS solution and stock solution for HPTS assay:

We have prepared a buffer solution using autoclaved water of strength 100 mM of NaCl and 10 mM of HEPES. The pH of the solution was below 7.0 and to make the pH at around 7.0 required amount of 0.5 M NaOH solution was added. Then 1 mM of HPTS solution was

prepared from solid HPTS using the above buffer solution. The stock solution for the HPTS assay was prepared from solid compound by using HPLC grade DMSO.

6.1.2. Preparation of vesicles for HPTS assay^{S10}

In a 10 mL round bottomed flask 1 mL of EYPC lipid solution (25 mg/mL in CHCl₃) was taken and the chloroform present in the lipid solution was evaporated by a slow stream of nitrogen gas to get a thin film of lipid. Then the trace amount of chloroform present in the lipid was evaporated by keeping it in high vacuum for about 4 h. The lipid membrane was then hydrated with 1 mL of HPTS solution (1 mM HPTS, 100 mM NaCl, 10 mM HEPES, pH 7.0) by vortexing 4-5 times over the time period of 1 h. Then the hydrated suspension was subjected through 20 freeze-thaw cycles and extrusions were done for 19 times (must be odd number) through 100 nm polycarbonate membrane. The extravesicular dyes were separated from vesicles by size exclusion column chromatography (Sephadex G-50) eluting with buffer solution (1 mM HPTS, 100 mM NaCl, 10 mM HEPES, pH 7.0). The vesicles were then diluted to 6 mL by using buffer (100 mM NaCl, 10 mM HEPES, pH 7.0) to get the concentration of 5.4 mM of EYPC-LUVs \supset HPTS, assuming no loss of lipid during gel filtration process. The vesicles contains, inside: 1 mM HPTS, 100 mM NaCl, 10 mM HEPES, pH 7.0 and outside: 100 mM NaCl, 10 mM HEPES, pH 7.0.

6.1.3. Ion transport study by HPTS assay

In a clean fluorimetric cuvette, 1975 μ L of buffer solution (100 mM NaCl, 10 mM HEPES, pH 7.0), 25 μ L of above prepared vesicles solution were taken and placed in a fluorescence instrument equipped with a magnetic stirrer at $t = 0$ s. The fluorescence emission intensity of the HPTS dye, I_t was measured at $\lambda_{em} = 510$ nm (where, $\lambda_{ex} = 450$ nm) for the time course of 0 to 350 s. At $t = 20$ s, 20 μ L of 0.5 M NaOH solution was added to the same cuvette to generate a pH gradient (Δ pH = 0.8) between intra and extra vesicular medium. Then 20 μ L solution of tripodal molecules in DMSO of different concentration were added at $t = 100$ s. At $t = 300$ s, 25 μ L of 10% triton X-100 was added to destroy all the vesicles for destructing the pH gradient.

The fractional emission intensity (in percentage), I_F (Fig. S14B) was obtained after normalizing all the data using the following equation (Eq. S3).

$$\% \text{ of } I_F = (I_t - I_0) / (I_\infty - I_0) \times 100 \quad \text{Eq. S3}$$

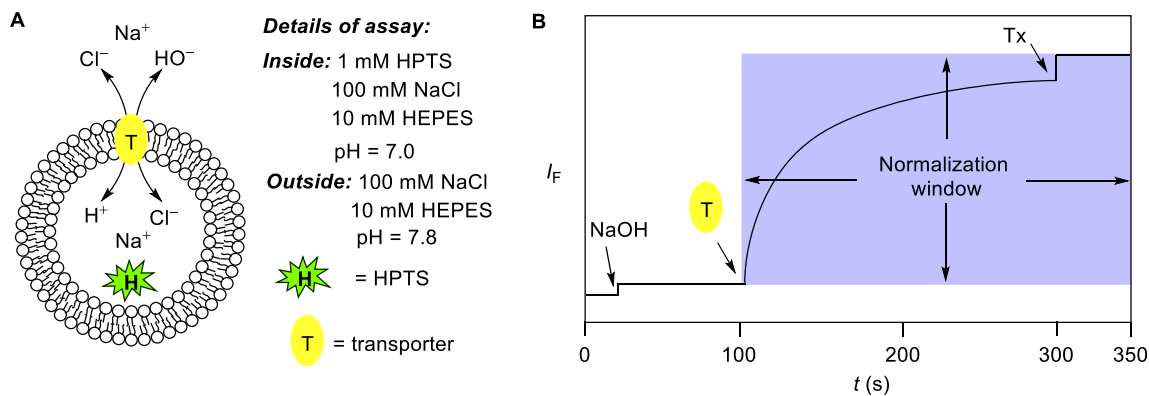


Fig. S14 Representation of fluorescence kinetics based HPTS assay for checking ion transport activity across EYPC-LUVs \supset HPTS (A), and normalization window for the same fluorescence kinetics experiment (B).

Where, I_0 is the fluorescence intensity just before the addition of the tripod compound, I_t is the fluorescence intensity at time t and I_∞ is the fluorescence intensity after the addition of Triton X-100.

For plotting all the data in to graph the time axis was normalized using the following equation:

$$t = t - 100 \tag{Eq. S4}$$

To get the relative activity for all the transporter molecules ion transport experiment was done across bilayer membrane using EYPC-LUVs \supset HPTS.

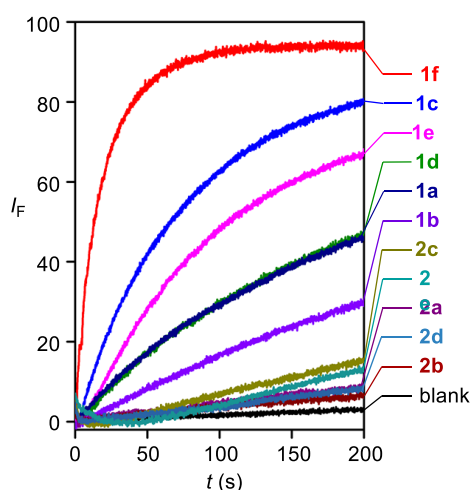


Fig. S15 Comparison of ion transport activities of all the transporter molecules (1a-f, 2a-e) across EYPC-LUVs \supset HPTS at 1 μ M transporter concentration.

The concentration profile data was used for fitting of the “Hill equation” (Eq. S5) to get the half maximal effective concentration (EC_{50}) and Hill coefficient (n).

$$Y = Y_{\infty} + (Y_0 - Y_{\infty}) / [(1 + (c / EC_{50})^n)] \quad \text{Eq. S5}$$

Where, Y_0 is the fluorescence intensity just before the addition of the tripodal compound, Y_{∞} is the fluorescence intensity after addition of excess tripodal compound, and c is the concentration of the compound.

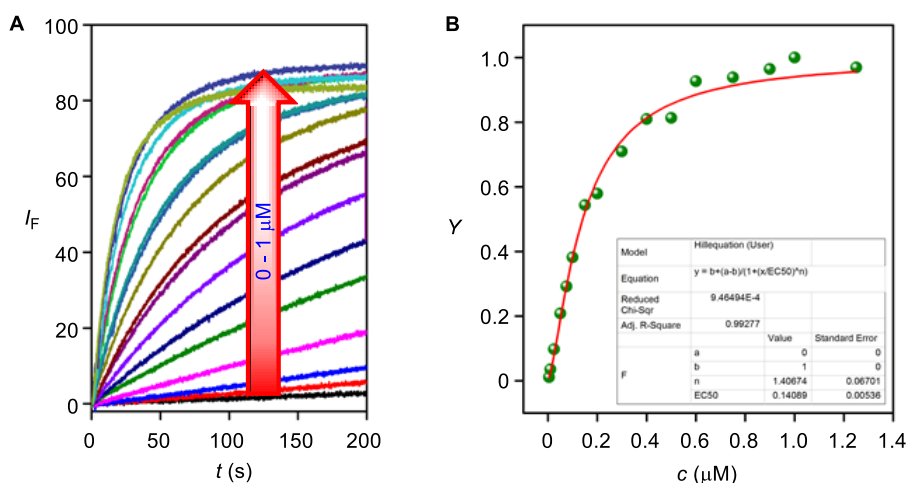


Fig. S16 Concentration dependent fluorescence kinetics based ion transport activity assay of compound **1f** (0–1 μM) across EYPC-LUVs \Rightarrow HPTS (A), and Hill plot of compound **1f** at $t = 100$ s to get EC_{50} and n (B).

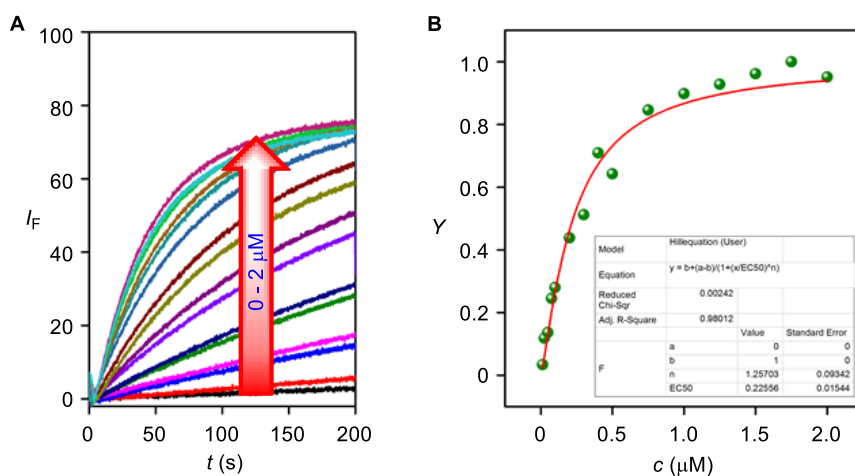


Fig. S17 Concentration dependent fluorescence kinetics based ion transport activity assay of compound **1c** (0–2 μM) across EYPC-LUVs \Rightarrow HPTS (A), and Hill plot of compound **1c** at $t = 100$ s to get EC_{50} and n (B).

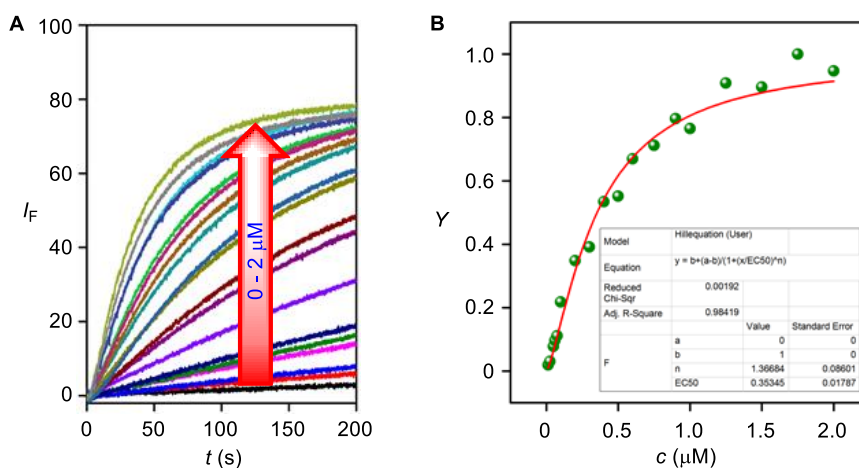


Fig. S18 Concentration dependent fluorescence kinetics based ion transport activity assay of compound **1e** (0–2 μM) across EYPC-LUVs \Rightarrow HPTS (A), and Hill plot of compound **1e** at $t = 100$ s to get EC_{50} and n (B).

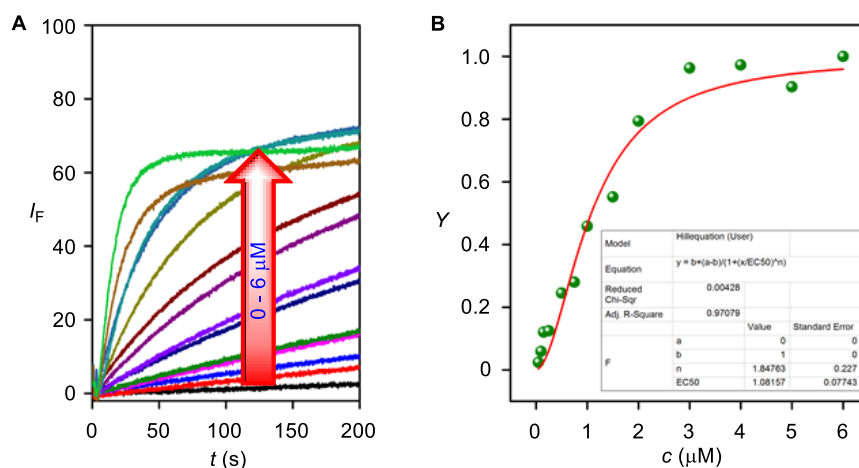


Fig. S19 Concentration dependent fluorescence kinetics based ion transport activity assay of compound **1d** (0–6 μM) across EYPC-LUVs \Rightarrow HPTS (A), and Hill plot of compound **1d** at $t = 100$ s to get EC_{50} and n (B).

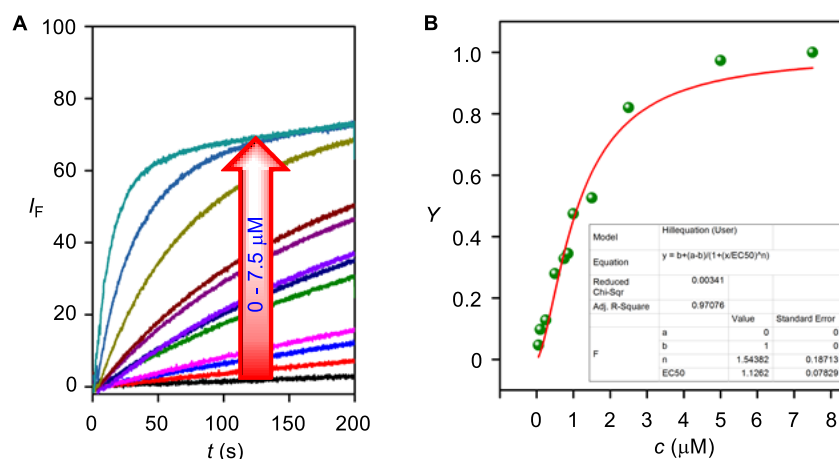


Fig. S20 Concentration dependent fluorescence kinetics based ion transport activity assay of compound **1a** (0–7.5 μM) across EYPC-LUVs \Rightarrow HPTS (A), and Hill plot of compound **1a** at $t = 100$ s to get EC_{50} and n (B).

6.2. Determination of Ion selectivity by HPTS assay

6.2.1. Preparation of buffer and stock solution for HPTS assay

We have prepared buffer solutions of different salts using autoclaved water of strength 100 mM of MX (where, MX = NaCl, NaBr, NaI, NaNO₃, NaSCN, NaClO₄, NaOAc, LiCl, KCl, RbCl, CsCl) and 10 mM of HEPES. The pH of the solutions were adjusted at around 7.0 by the addition of required amount of 0.5 M NaOH solution. Then 1 mM of HPTS solution was prepared from solid HPTS using the above buffer solution. The stock solution for the HPTS assay was prepared from solid compound by using HPLC grade DMSO.

6.2.2. Preparation of vesicles for ion selectivity by HPTS assay

The vesicles for the ion selectivity assay was prepared following the same procedure as mentioned earlier.

6.2.3. Cation selectivity transport study by HPTS assay

In a clean fluorimetric cuvette, 1975 μL of buffer solution (100 mM MCl, 10 mM HEPES, pH 7.0; where, $\text{M}^+ = \text{Li}^+, \text{Na}^+, \text{K}^+, \text{Rb}^+, \text{and Cs}^+$), 25 μL of above prepared vesicles solution were taken and placed in a fluorescence instrument equipped with a magnetic stirrer at $t = 0$ s. The fluorescence emission intensity of the HPTS dye, I_t was measured at $\lambda_{\text{em}} = 510$ nm (where $\lambda_{\text{ex}} = 450$ nm) for the time course of 0 to 350 s. At $t = 20$ s, 20 μL of 0.5 M NaOH solution was added to the same cuvette to generate a pH gradient ($\Delta\text{pH} = 0.8$) between intra and extra vesicular medium. Then 20 μL solution of tripodal molecules in DMSO was added at $t = 100$ s. At $t = 300$ s, 25 μL of 10% triton X-100 was added to destroy all the vesicles for destructing the pH gradient. All the data was normalized using the Eq. S3 and Eq. S4.

6.2.4. Anion selectivity transport study by HPTS assay

In a clean fluorimetric cuvette, 1975 μL of buffer solution (100 mM NaX, 10 mM HEPES, pH 7.0; where, $\text{X}^- = \text{Cl}^-, \text{Br}^-, \text{I}^-, \text{NO}_3^-, \text{SCN}^-, \text{ClO}_4^-, \text{and AcO}^-$), 25 μL of above prepared vesicles solution were taken and placed in a fluorescence instrument equipped with a magnetic stirrer at $t = 0$ s. The fluorescence emission intensity of the HPTS dye, I_t was measured at $\lambda_{\text{em}} = 510$ nm (where $\lambda_{\text{ex}} = 450$ nm) for the time course of 0 to 350 s. At $t = 20$ s, 20 μL of 0.5 M NaOH solution was added to the same cuvette to generate a pH gradient ($\Delta\text{pH} = 0.8$) between intra and extra vesicular medium. Then 20 μL solution of tripodal molecules in DMSO of different concentration were added at $t = 100$ s. At $t = 300$ s, 25 μL of 10% triton X-100 was added to destroy all the vesicles for destructing the pH gradient. All the data was normalized using the Eq. S3 and Eq. S4

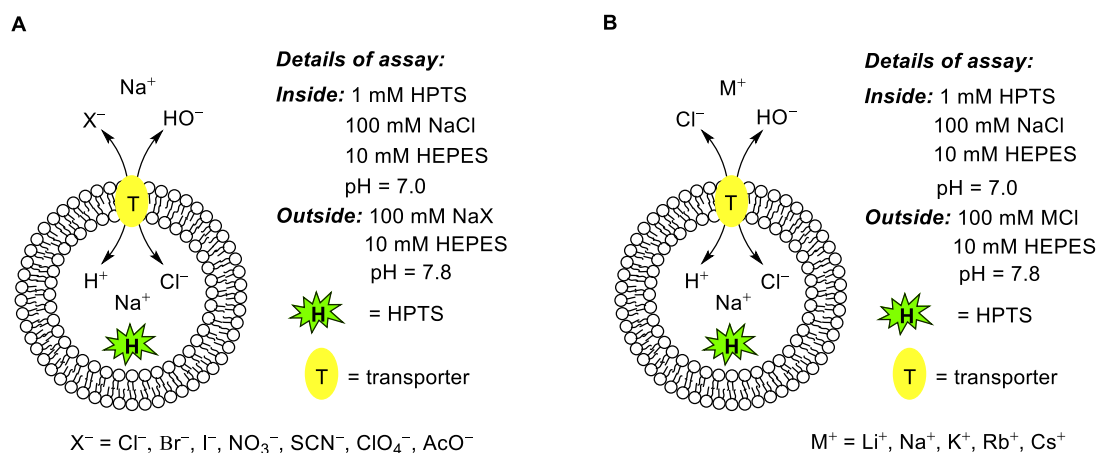


Fig. S21 Representation of fluorescence kinetics based HPTS assay for checking ion selectivity across EYPC-LUVs \Rightarrow HPTS. Anion selectivity assay (A), and cation selectivity assay (B).

6.3. Ion transport mechanism study by HPTS assay

6.3.1. Preparation of buffer and stock solution for FCCP and valinomycin assay

We have prepared a buffer solution using autoclaved water of strength 100 mM of NaCl and 10 mM of HEPES. The pH of the solution was adjusted at around 7.0 by the addition of required amount of 0.5 M NaOH solution. Then 1 mM of HPTS solution was prepared from solid HPTS using the above buffer solution. We have prepared another buffer solution for valinomycin assay using autoclaved water of strength 100 mM of KCl and 10 mM of HEPES. The stock solution of **1a**, FCCP, and valinomycin for the HPTS assay was prepared from solid compound by using HPLC grade DMSO.

6.3.2. Preparation of vesicles for FCCP and Valinomycin assay

The vesicles for the FCCP assay was prepared following the same procedure as mentioned earlier.

6.3.3. Ion transport activity study in presence of FCCP

In a clean fluorimetric cuvette, 1975 μ L of buffer solution (100 mM NaCl, 10 mM HEPES, pH 7.0), 25 μ L of above prepared vesicles solution were taken and placed in a fluorescence instrument equipped with a magnetic stirrer at $t = 0$ s. The fluorescence emission intensity of the HPTS dye, I_t was measured at $\lambda_{em} = 510$ nm (where $\lambda_{ex} = 450$ nm) for the time course of 0 to 350 s. At $t = 20$ s, 20 μ L of 0.5 M NaOH solution was added to the same cuvette to generate a pH gradient (Δ pH = 0.8) between intra and extra vesicular medium. Then FCCP (2.5 μ M) was added at $t = 50$ s followed by the addition of 20 μ L solution of tripodal

molecule in DMSO at $t = 100$ s. At $t = 300$ s, 25 μL of 10% triton X-100 was added to destroy all the vesicles for destructing the pH gradient. All the data was normalized using the Eq. S3 and Eq. S4.

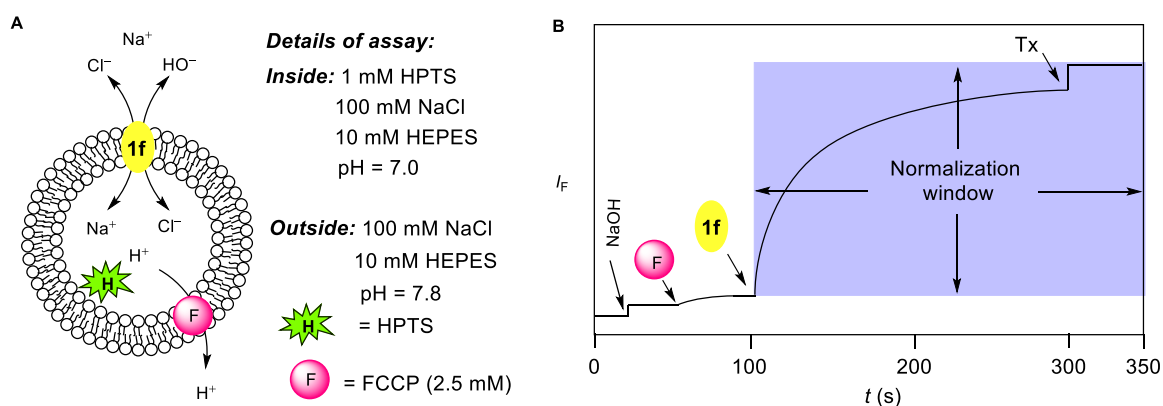


Fig. S22 Representation of fluorescence kinetics based HPTS assay for checking ion transport activity in presence of FCCP across EYPC-LUVs \Rightarrow HPTS (A), and normalization window for the same fluorescence kinetics experiment (B).

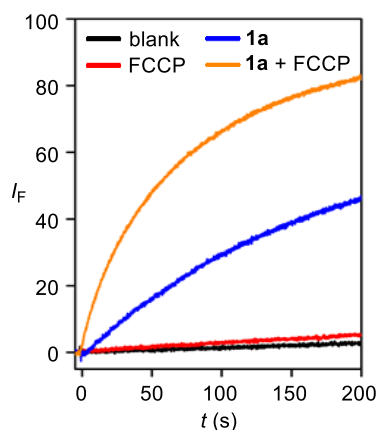


Fig. S23 Ion transport activity of **1f** (0.16 μM) determined in the absence and presence of FCCP.

6.3.4. Ion transport activity study in presence of valinomycin

In a clean fluorimetric cuvette 1975 μL of buffer solution (100 mM KCl, 10 mM HEPES, pH 7.0), 25 μL of above prepared vesicles solution were taken and placed in a fluorescence instrument equipped with a magnetic stirrer at $t = 0$ s. The fluorescence emission intensity of the HPTS dye, I_t was measured at $\lambda_{em} = 510$ nm (where $\lambda_{ex} = 450$ nm) for the time course of 0 to 350 s. At $t = 20$ s, 20 μL of 0.5 M NaOH solution was added to the same cuvette to generate a pH gradient ($\Delta\text{pH} = 0.8$) between intra and extra vesicular medium. Then valinomycin (2.5 pM) was added at $t = 50$ s followed by the addition of 20 μL solution of tripodal molecule (0.16 μM) in DMSO at $t = 100$ s. At $t = 300$ s, 25 μL of 10% triton X-100

was added to destroy all the vesicles for destructing the pH gradient. All the data was normalized using the Eq. S3 and Eq. S3.

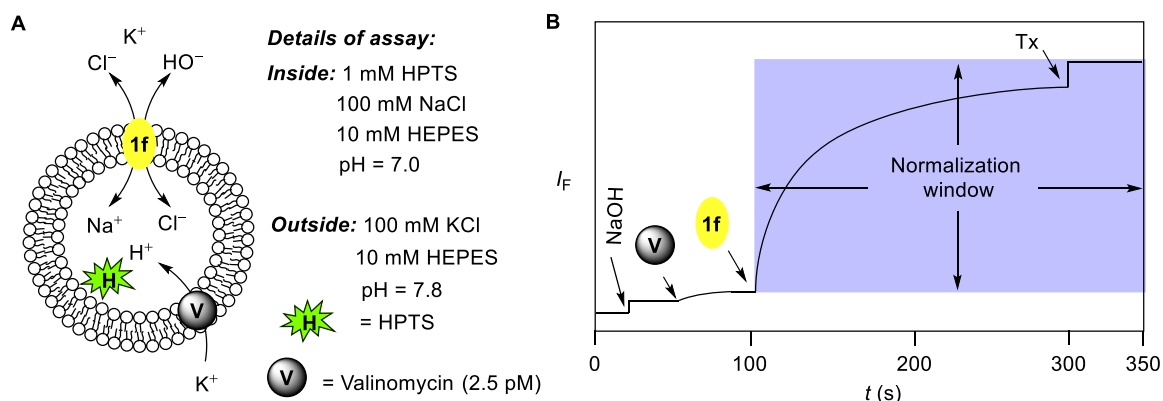


Fig. S24 Representation of fluorescence kinetics based HPTS assay for checking ion transport activity in presence of valinomycin across EYPC-LUVs \Rightarrow HPTS (A), and normalization window for the same fluorescence kinetics experiment (B).

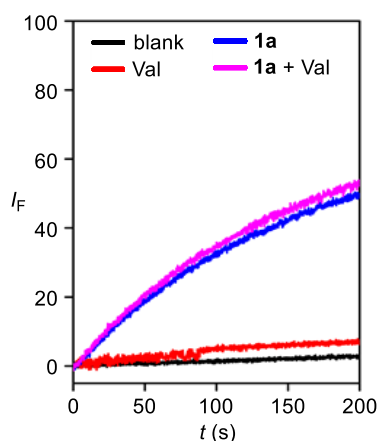


Fig. S25 Ion transport activity of **1f** (0.16 μM) determined in the absence and presence of valinomycin.

6.4. Determination of Cl^- transport activity by Lucigenin assay

6.4.1. Preparation of Salt solution and Stock for Lucigenin assay

We have prepared a salt solution using autoclaved water of strength 225 mM of NaNO_3 . Then 1 mM of Lucigenin solution was prepared from solid Lucigenin using the above solution. The stock solution of the compound for the Lucigenin assay was prepared from solid compound by using HPLC grade $\text{CH}_3\text{CN} : \text{CH}_3\text{OH} = 5 : 1$.

6.4.2. Preparation of vesicles for Lucigenin assay

In a 10 mL round bottomed flask 1 mL of EYPC lipid solution (25 mg/mL in CHCl_3) was taken and the chloroform present in the lipid solution was evaporated by a slow stream of

nitrogen gas to get a thin film of lipid. Then the trace amount of chloroform present in the lipid was evaporated by keeping it in high vacuum for about 4 h. The lipid membrane was then hydrated with 1 mL of Lucigenin solution (1 mM Lucigenin, 225 mM NaNO₃) by vortexing 4-5 times over the time period of 1 h. Then the hydrated suspension was subjected through 20 freeze-thaw cycles and extrusions were done for 19 times through 200 nm polycarbonate membrane. The extravesicular Lucigenin dyes were separated from vesicles by size exclusion column chromatography (Sephadex G-50) using 225 mM of NaNO₃ solution. The vesicles were then diluted to 4 mL by using the same 225 mM of NaNO₃ solution to get the concentration of ~ 8 mM of EYPC-LUVs \supset Lucigenin, assuming no loss of lipid during gel filtration process. The vesicles contains, inside: 1 mM Lucigenin, 225 mM NaNO₃ and outside: 225 mM NaNO₃.

6.4.3. Concentration dependent Cl⁻ transport by lucigenin assay

In a clean fluorimetric cuvette 1950 μ L of 225 mM NaNO₃ solution, 25 μ L of above prepared vesicles solution were taken and placed in a fluorescence instrument equipped with a magnetic stirrer at $t = 0$ s. The fluorescence emission intensity of the Lucigenin dye, I_t was measured at $\lambda_{em} = 535$ nm (where, $\lambda_{ex} = 455$ nm) for the time course of 0 to 350 s. At $t = 20$ s, 33.3 μ L of 2N NaCl solution was added to the same cuvette to generate a chloride ion concentration gradient between intra and extravesicular medium. Then 20 μ L solution of tripodal molecule of different concentration were added at $t = 100$ s. At $t = 300$ s, 25 μ L of 10% triton X-100 was added to destroy all the vesicles for destructing the chloride ion concentration gradient.

The fractional emission intensity, I_F (Fig. S26B) was obtained after normalizing all the data using the following equation (Eq. S6).

$$\% \text{ of } I_F = (I_t - I_0) / (I_\infty - I_0) \times (-100) \quad \text{Eq. S6}$$

Where, I_0 is the fluorescence intensity just before the addition of the tripodal compound, I_t is the fluorescence intensity at time t , and I_∞ is the fluorescence intensity after the addition of Triton X-100.

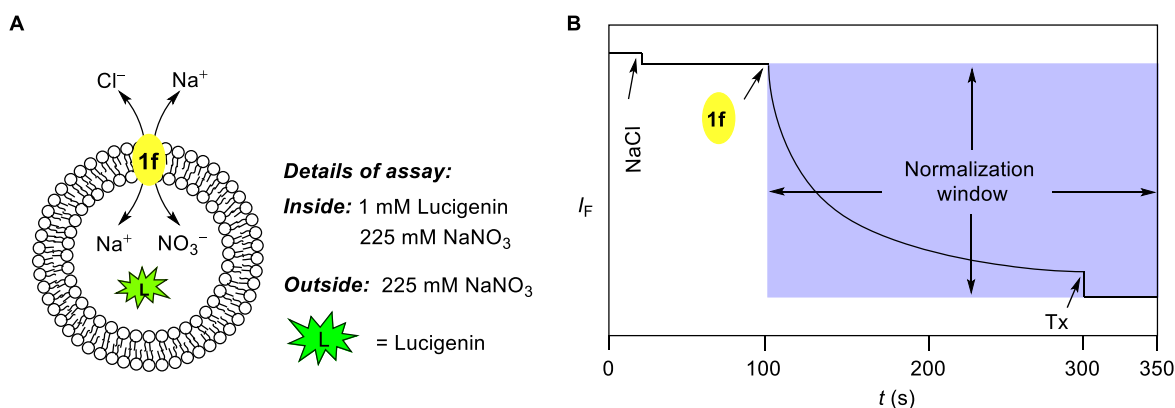


Fig. S26 Representation of fluorescence kinetics based Lucigenin assay for checking the chloride ion transport activity across EYPC-LUVs \Rightarrow Lucigenin (A), and normalization window for the same fluorescence kinetics experiment (B).

For plotting all the data in to graph the time axis was normalized using Eq. S4, The concentration profile data was used for fitting of the “Hill equation” (Eq. S5) to get the half maximal effective concentration (EC_{50}) and Hill coefficient (n).

Where, Y_0 is the fluorescence intensity just before the addition of the tripodal compound, Y_∞ is the fluorescence intensity after addition of excess tripodal compound, and c is the concentration of the compound.

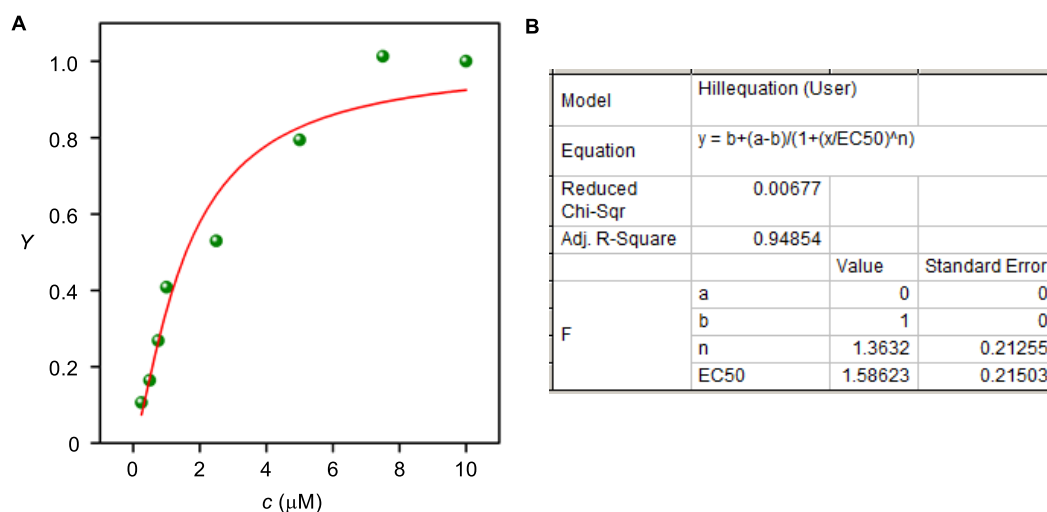


Fig. S27 Hill plot of compound **1f** at $t = 100$ s to get EC_{50} and n (A) and table for Hill equation (B).

6.4.4. Cl⁻ transport by Symport assay in presence of Lucigenin

In a clean fluorimetric cuvette 1950 μ L of 225 mM NaNO₃ solution, 25 μ L of above prepared vesicles solution were taken and placed in a fluorescence instrument equipped with a magnetic stirrer at $t = 0$ s. The fluorescence emission intensity of the Lucigenin dye, I_t was measured at $\lambda_{em} = 535$ nm (where $\lambda_{ex} = 455$ nm) for the time course of 0 to 350 s. At $t = 50$ s, 33.3 μ L of 2 N MCl (where, $M^+ = Li^+, Na^+, K^+, Rb^+, \text{ and } Cs^+$) solution was added to the same

cuvette to generate a concentration gradient of ions (Cl^- and M^+) between intra and extra vesicular medium. Then 20 μL of 0.15 mM tripodal molecule was added at $t = 100$ s and at, $t = 300$ s, 25 μL of 10% triton X-100 was added to destroy all the vesicles for destructing the chloride ion concentration gradient.

The fractional emission intensity (in percentage), I_F (Fig. S28B) was obtained after normalizing all the data using the equation Eq. S6 and for plotting all the data in to graph, the time axis was normalized using Eq. S4.

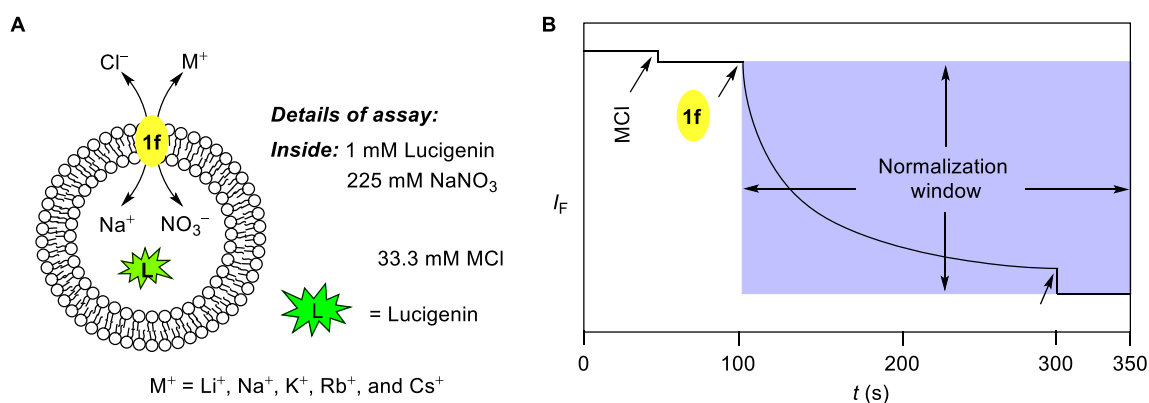


Fig. S28 Representation of fluorescence kinetics based symport assay using EYPC-LUVs with Lucigenin (A), and normalization window for the same fluorescence kinetics experiment (B)

6.4.5. Cl^- transport by Lucigenin assay in presence of Valinomycin

In a clean fluorimetric cuvette 1950 μL of 225 mM NaNO_3 solution, 25 μL of above prepared vesicles solution were taken and placed in a fluorescence instrument equipped with a magnetic stirrer at $t = 0$ s. The fluorescence emission intensity of the Lucigenin dye, I_t was measured at $\lambda_{\text{em}} = 535$ nm (where, $\lambda_{\text{ex}} = 455$ nm) for the time course of 0 to 350 s. At $t = 20$ s, 33.3 μL of 2 N KCl solution was added to the same cuvette to generate a concentration gradient of ions (Cl^- and K^+) between intra and extra vesicular medium. Then valinomycin (0.5 μM) was added at $t = 50$ s followed by the addition of 20 μL of 75 μM solution of tripodal molecule at $t = 100$ s and at, $t = 300$ s, 25 μL of 10% triton X-100 was added to destroy all the vesicles for destructing the chloride ion concentration gradient.

The fractional emission intensity (in percentage), I_F (Fig. S29B) was obtained after normalizing all the data using the equation Eq. S6 and for plotting all the data in to graph, the time axis was normalized using Eq. S4.

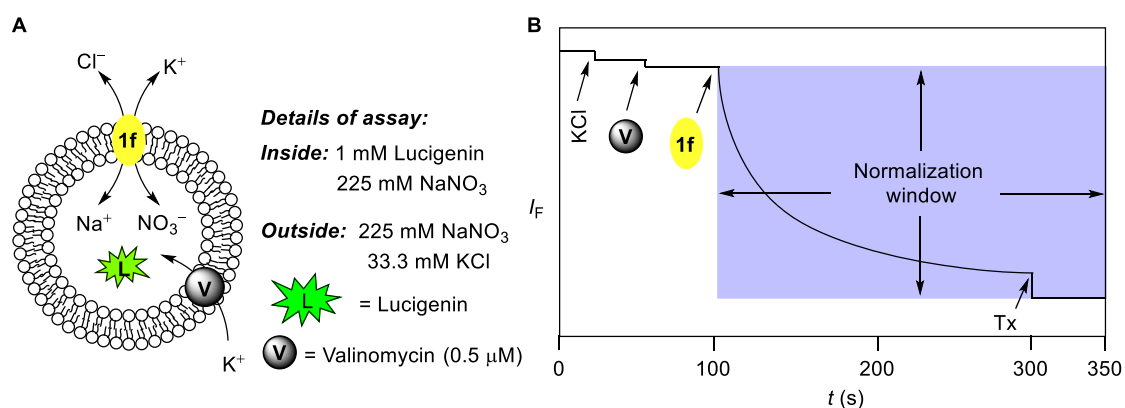


Fig. S29 Representation of fluorescence kinetics based Lucigenin assay in presence of Valinomycin using EYPC-LUVs \supset Lucigenin (A), and normalization window for the same fluorescence kinetics experiment (B).

6.5. U-tube experiments for checking Cl⁻ transport

In this experiment we have checked whether the chloride ion is transporting *via* mobile carrier mechanism or ion channel formation by transporter molecule. For that we have set up an experiment using an U-tube where left arm (Source arm) of the tube was filled with 7.5 mL of 500 mM NaCl solution buffered to pH 7.0 using 5mM phosphate buffer and the right arm (receiver arm) of the tube was filled with 7.5 mL of 500 mM NaNO₃ solution buffered to pH 7.0 using 5mM phosphate buffer. Two different salts solution in two different arm were separated by 15 mL solution of compound **1f** in CHCl₃ (1 mM compound **1f**, 1 mM tetrabutylammonium hexafluorophosphate) in such a way that two salts solution never come contact with each other. Here transport of chloride ion is only possible *via* mobile carrier mechanism due to the long length of CHCl₃ layer, which does not allow the formation ion channel. For checking transport activity via carrier mechanism chloride ion concentration in the receiver arm was measured by chloride ion selective electrode. The gradual increase of chloride ion concentration (Fig. S30) was measured in a fixed time interval for the time period of 8 days, gave evidence in support of mobile carrier mechanism. In a control experiment no increase in chloride ion concentration was observed when we omitted transporter molecule **1f** keeping other conditions same.

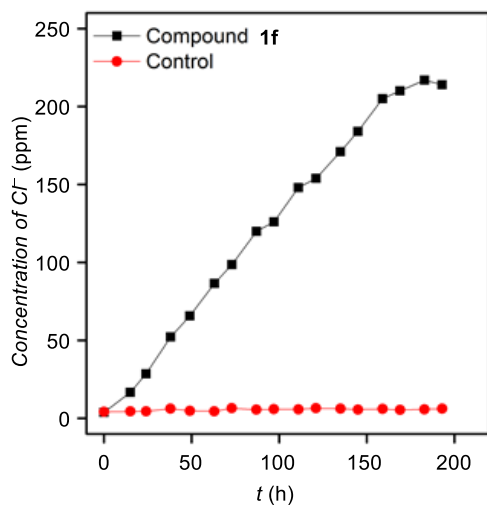


Fig. S30 Change of chloride ion concentration in U-tube experiment with and without using compound **1f** (1 mM).

7. NMR spectra of Compounds.

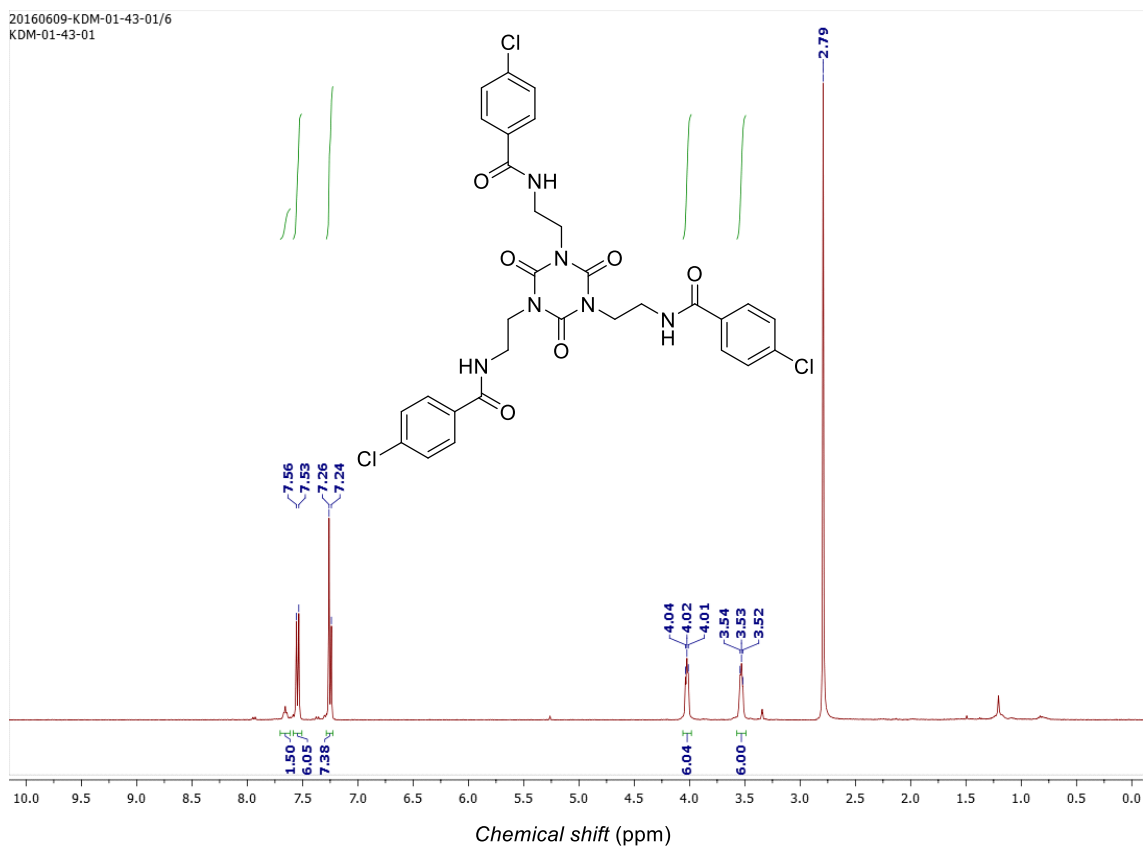


Fig. S31 ^1H NMR spectrum of compound **1a** in $\text{CDCl}_3:\text{MeOH-}d_4 = 4:1$.

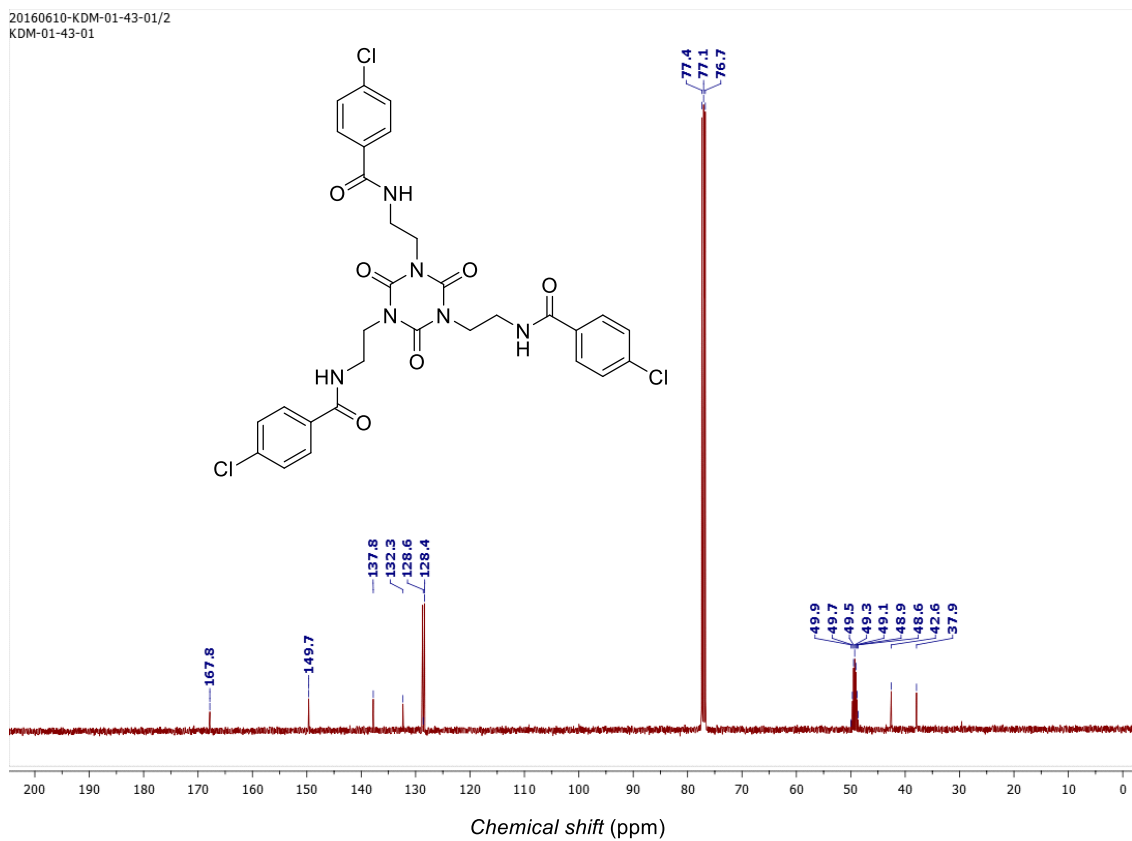


Fig. S32 ^{13}C NMR spectrum of compound **1a** in $\text{CDCl}_3:\text{MeOH-}d_4 = 4:1$.

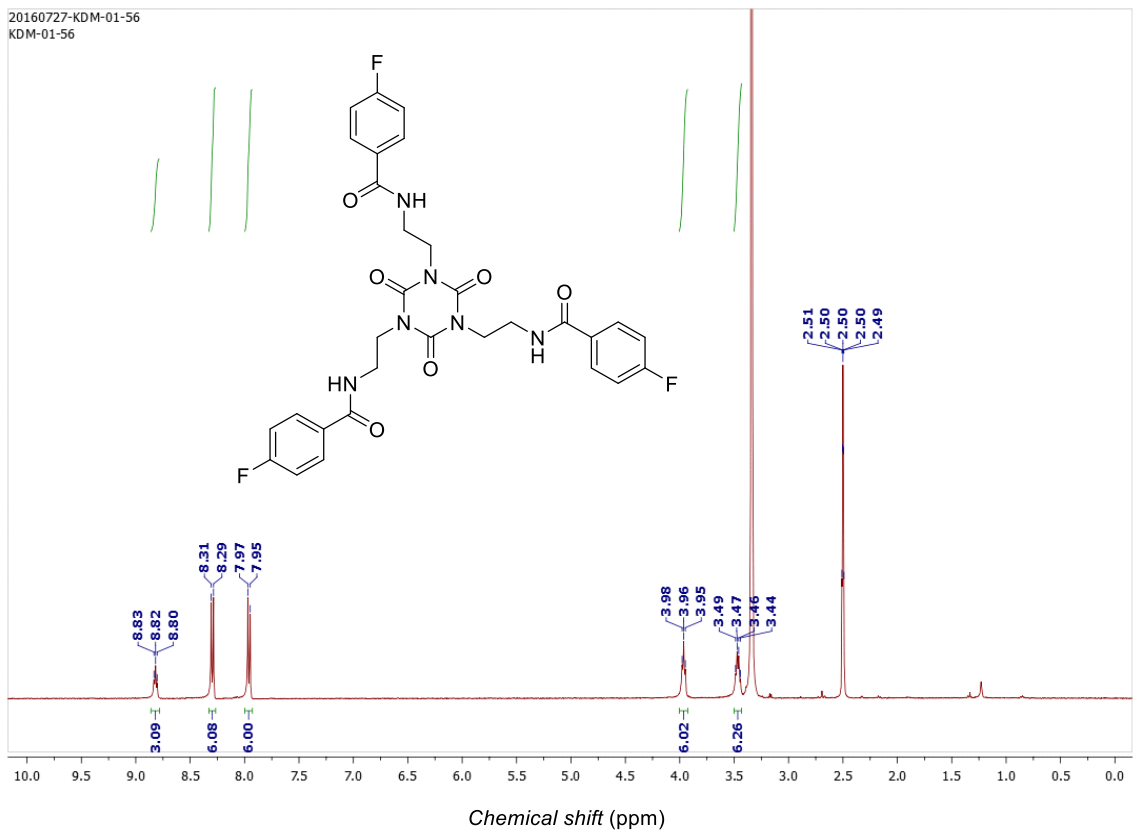


Fig. S33 ^1H NMR spectrum of compound **1b** in $\text{DMSO-}d_6$.

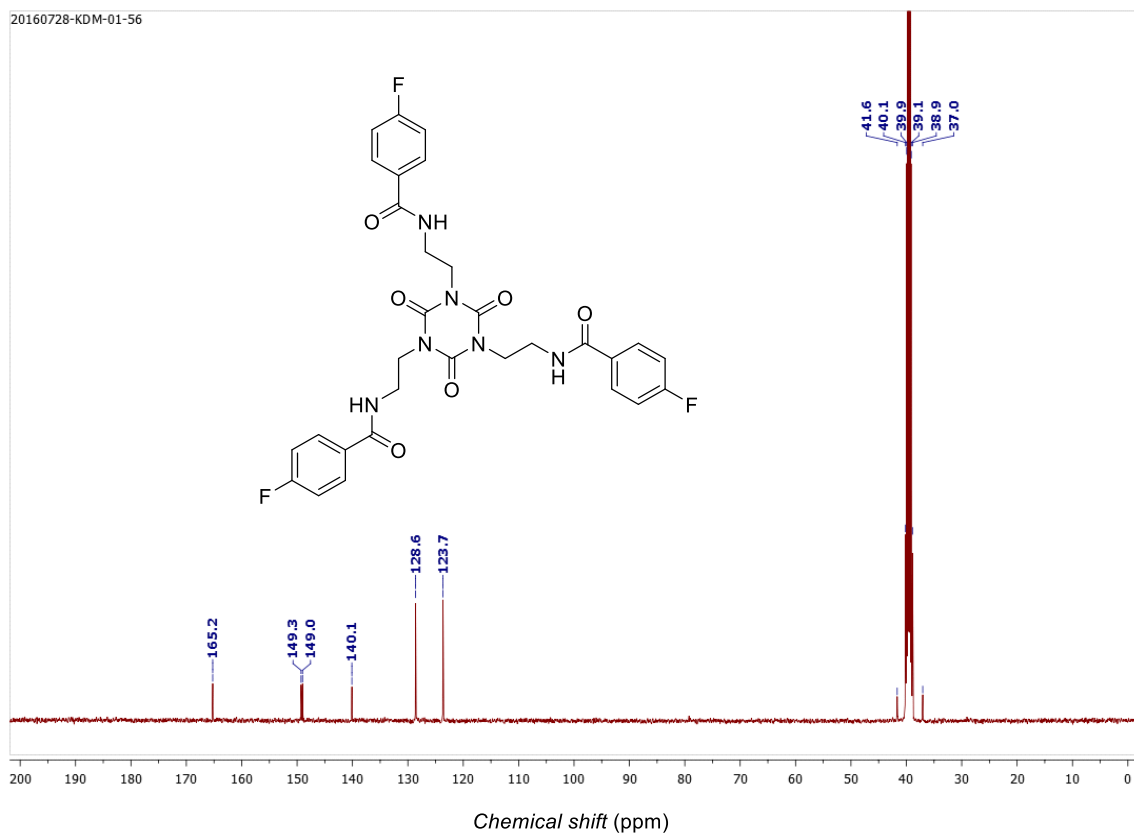


Fig. S34 ^{13}C NMR spectrum of compound **1b** in $\text{DMSO-}d_6$.

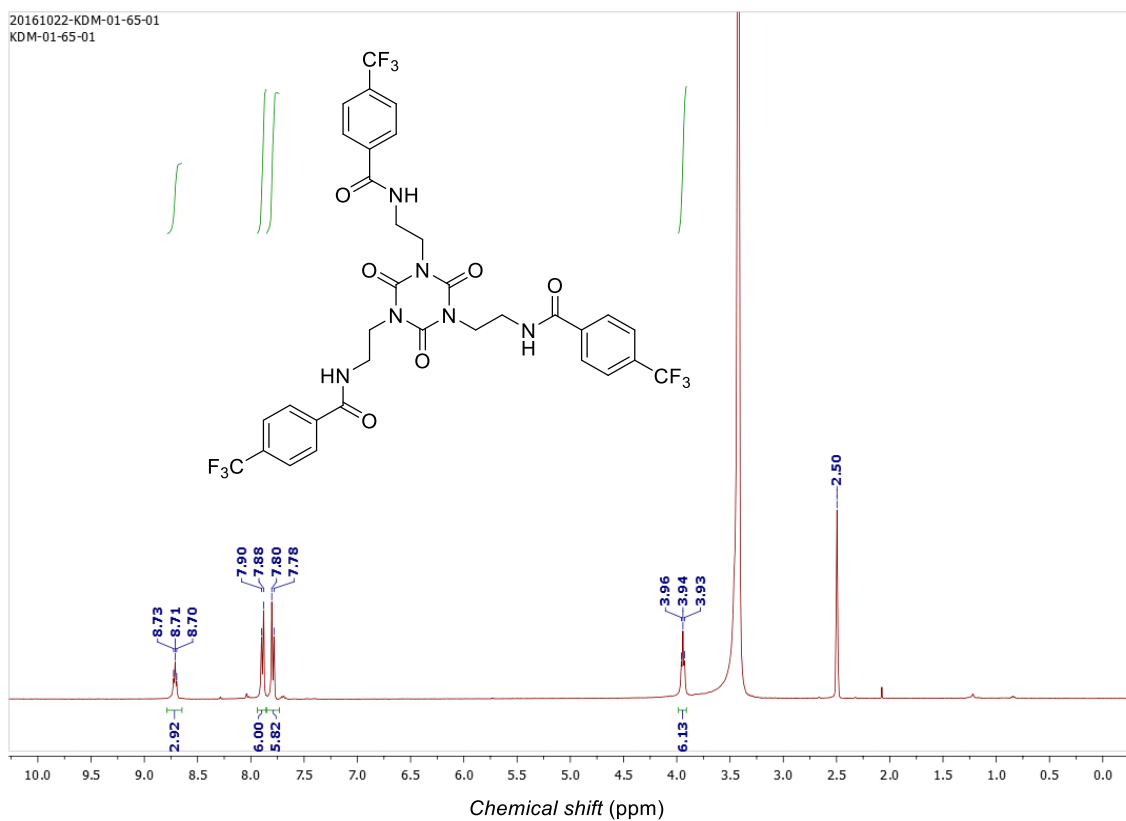


Fig. S35 ^1H NMR spectrum of compound **1c** in $\text{DMSO-}d_6$.

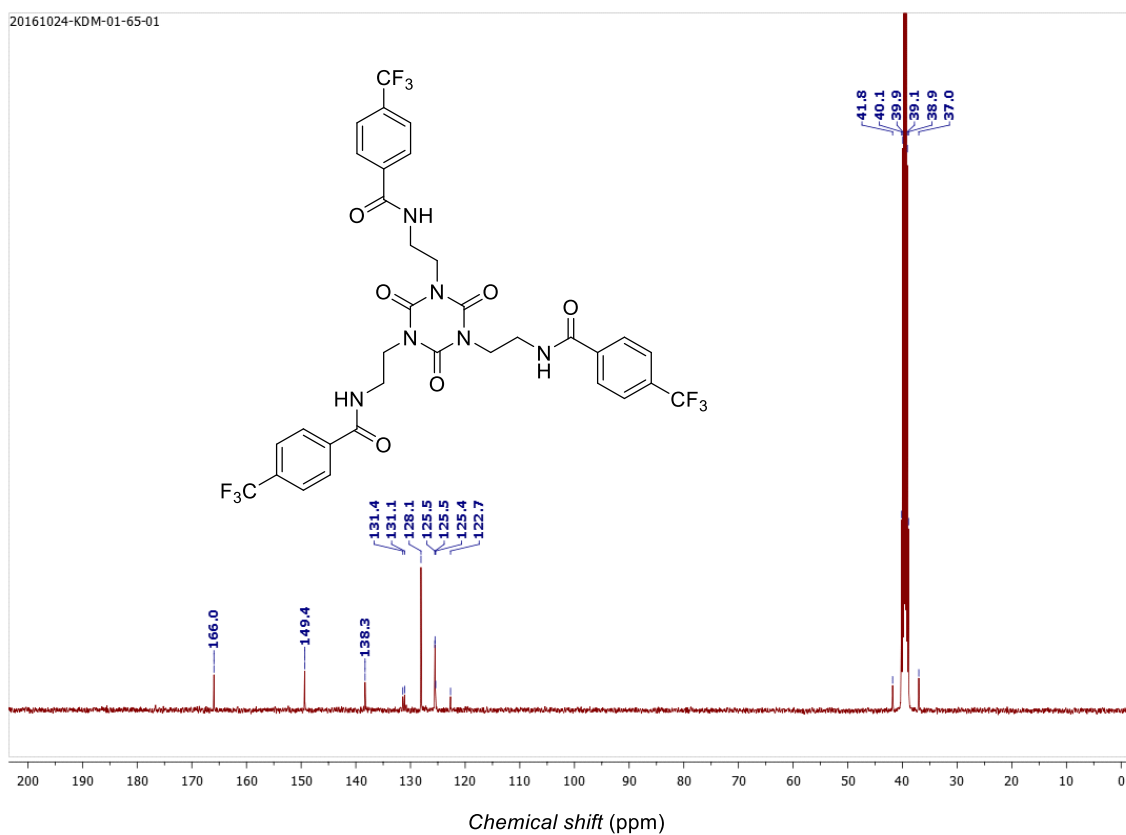


Fig. S36 ^{13}C NMR spectrum of compound **1c** in $\text{DMSO-}d_6$.

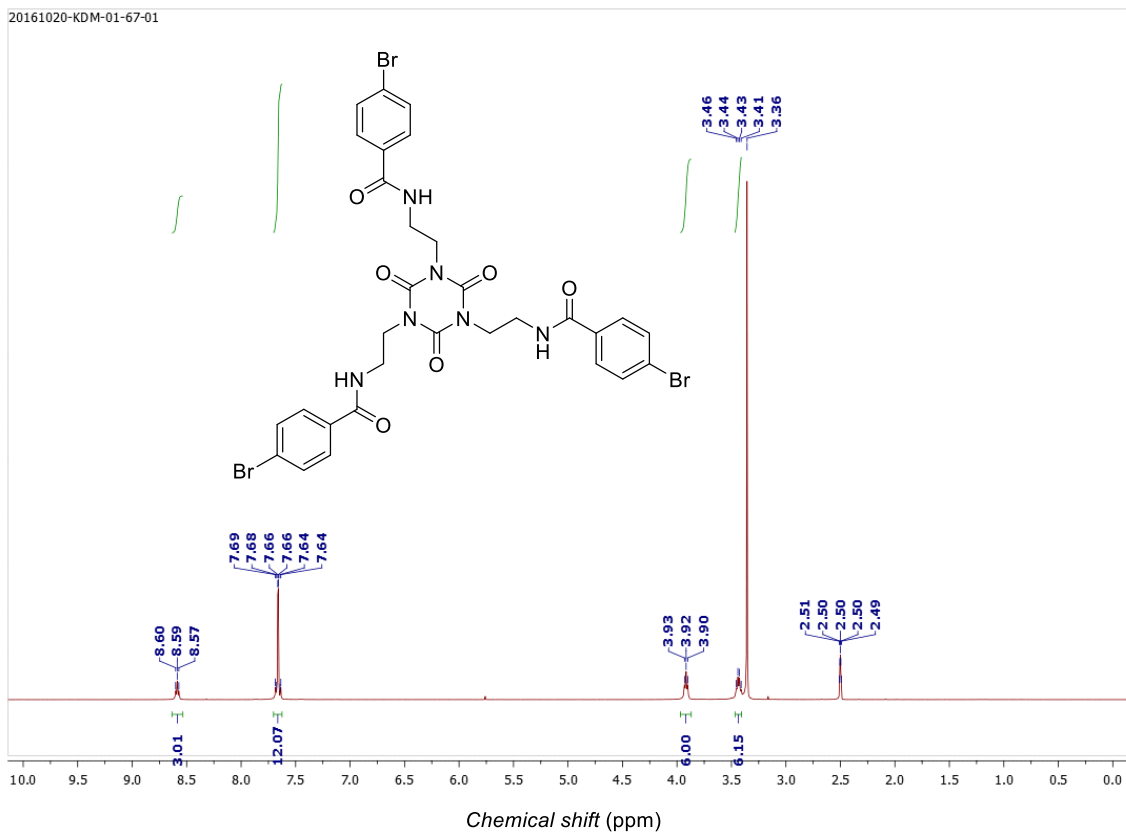


Fig. S37 ^1H NMR spectrum of compound **1d** in $\text{DMSO-}d_6$.

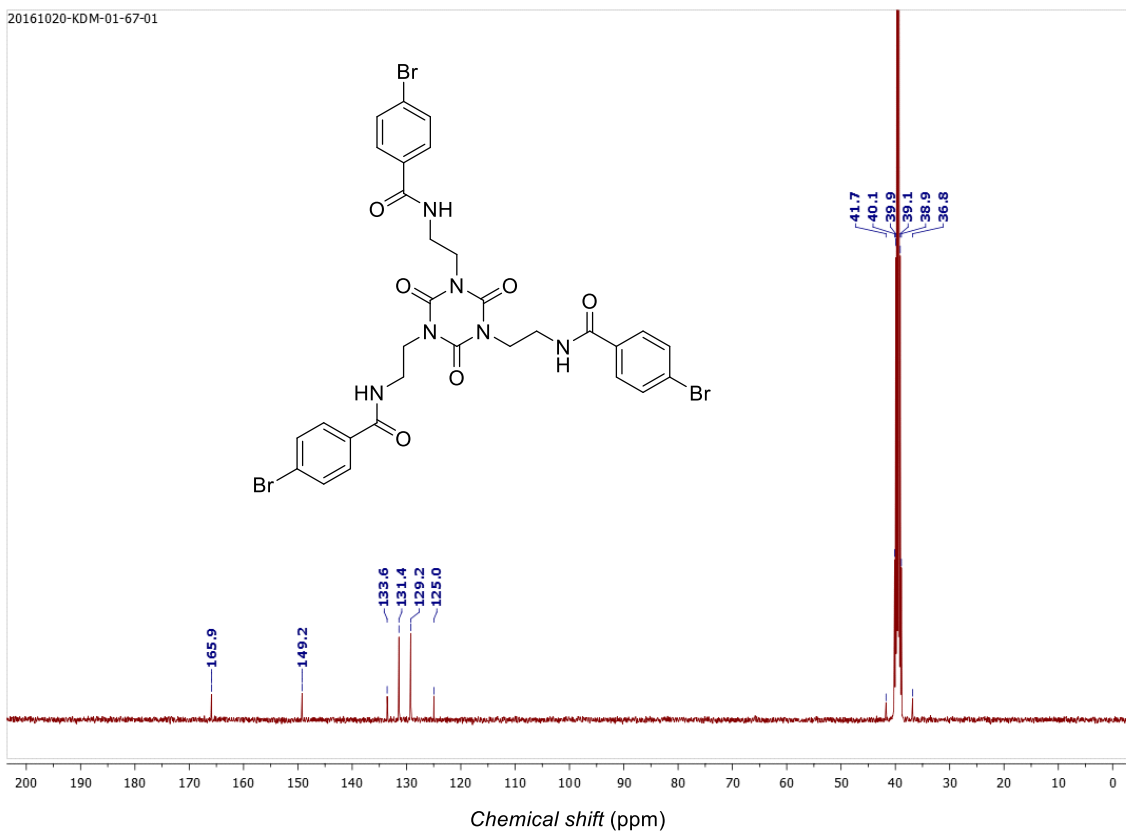


Fig. S38 ^{13}C NMR spectrum of compound **1d** in $\text{DMSO-}d_6$.

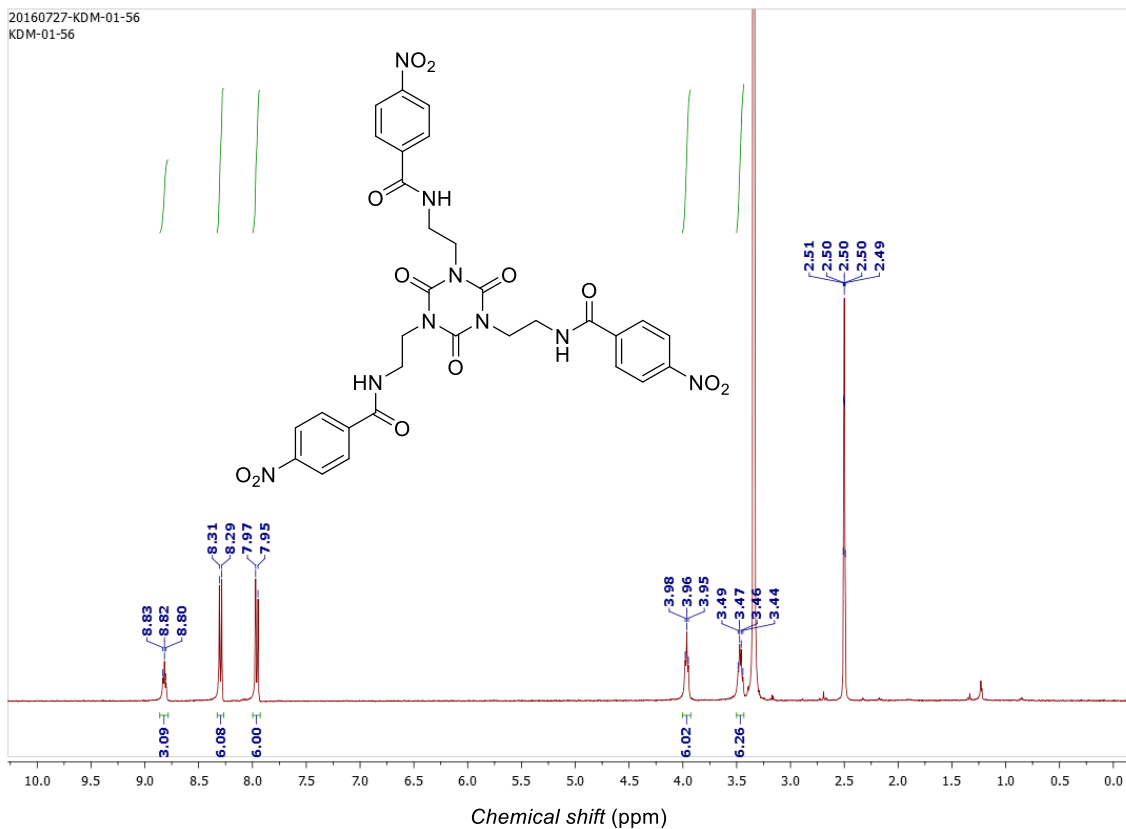


Fig. S39 ^1H NMR spectrum of compound **1e** in $\text{DMSO-}d_6$.

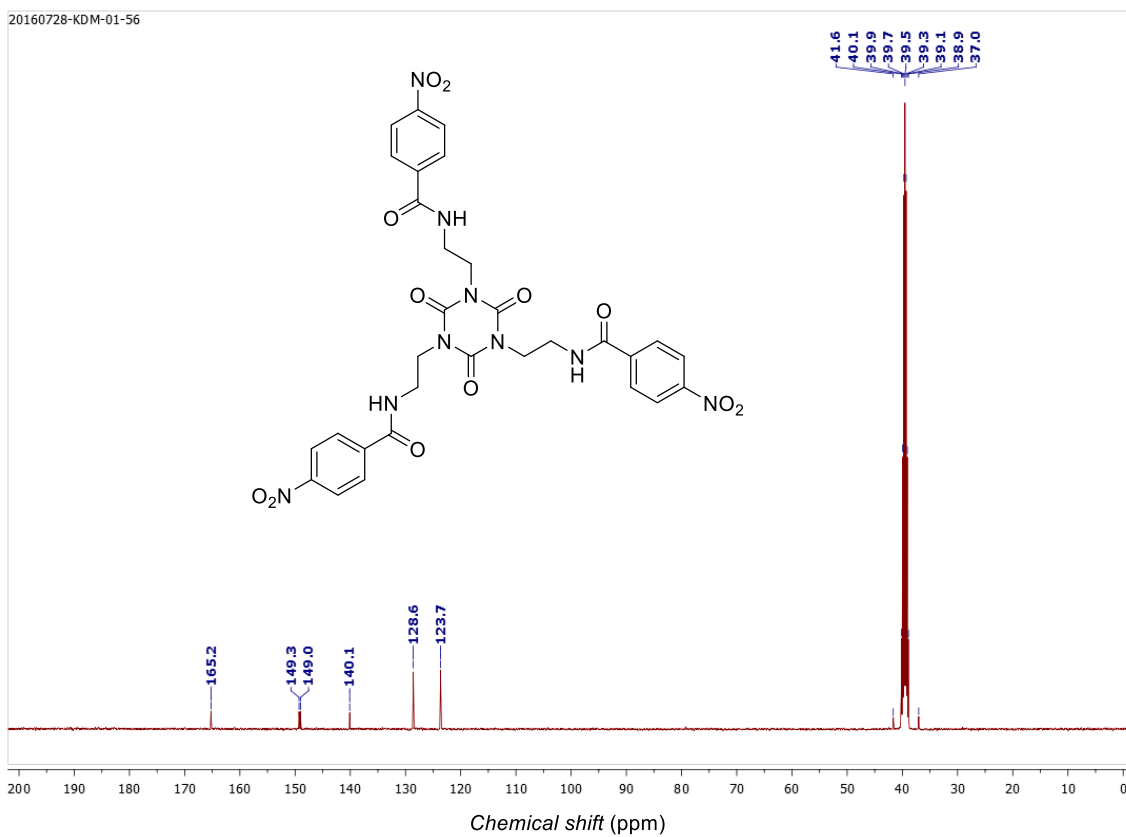


Fig. S40 ^{13}C NMR spectrum of compound **1e** in $\text{DMSO-}d_6$.

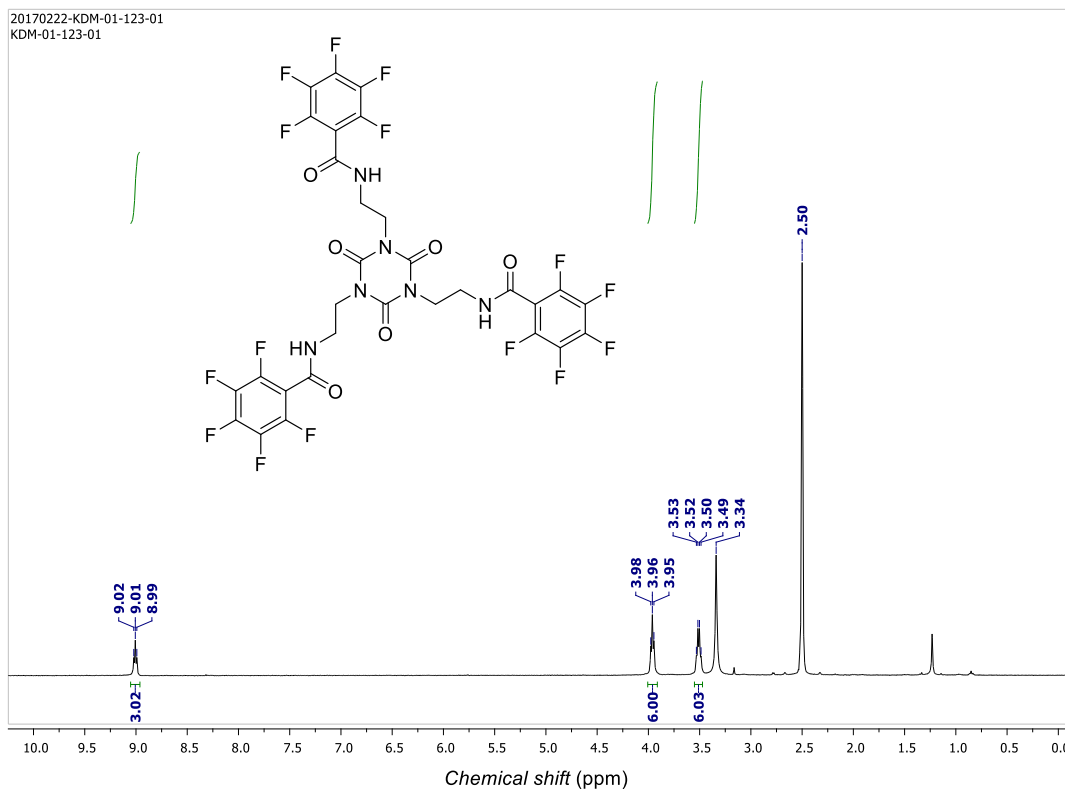


Fig. S41 ^1H NMR spectrum of compound **1f** in $\text{DMSO-}d_6$.

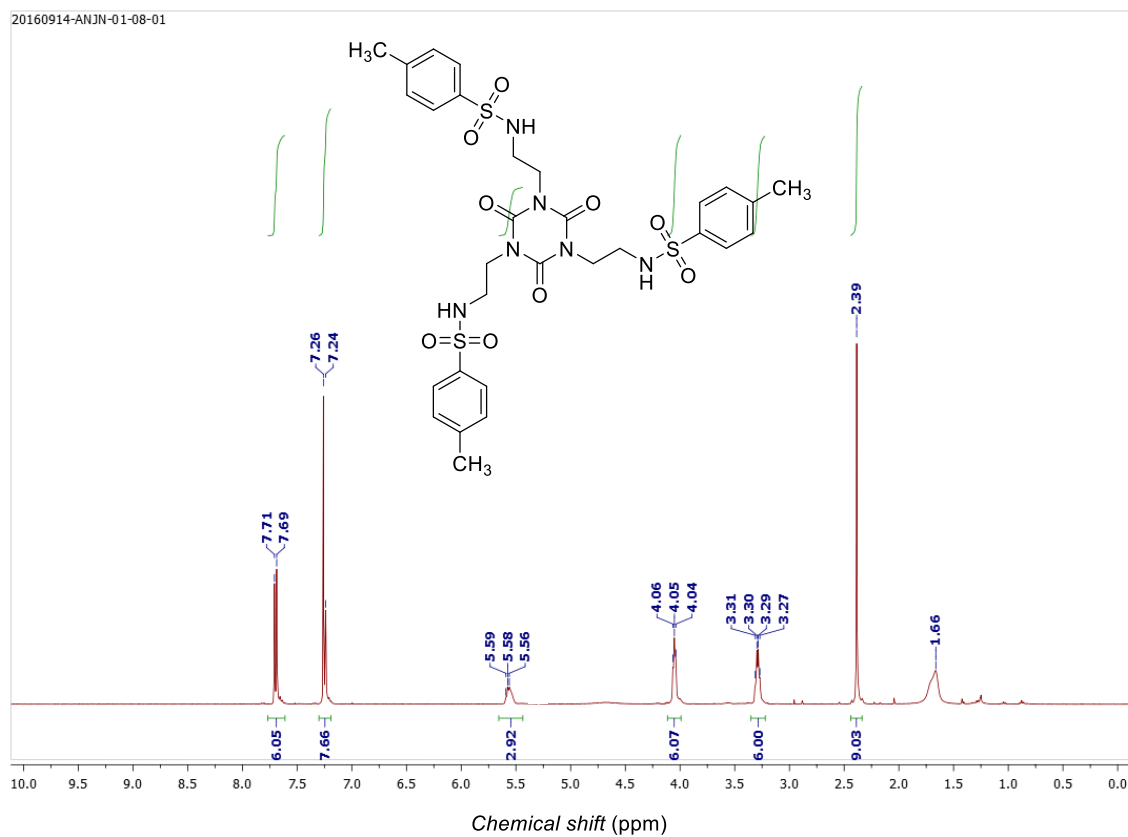


Fig. S42 ^1H NMR spectrum of compound **2a** in CDCl_3 .

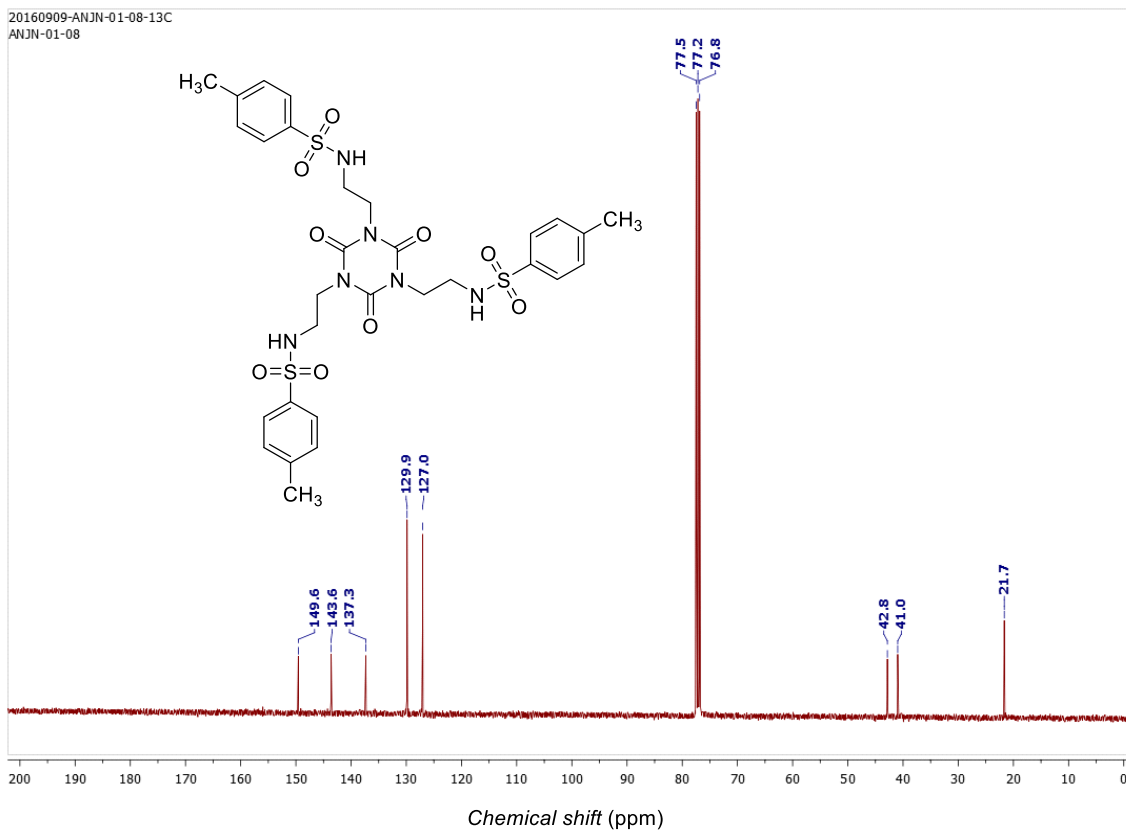


Fig. S43 ^{13}C NMR spectrum of compound **2a** in CDCl_3 .

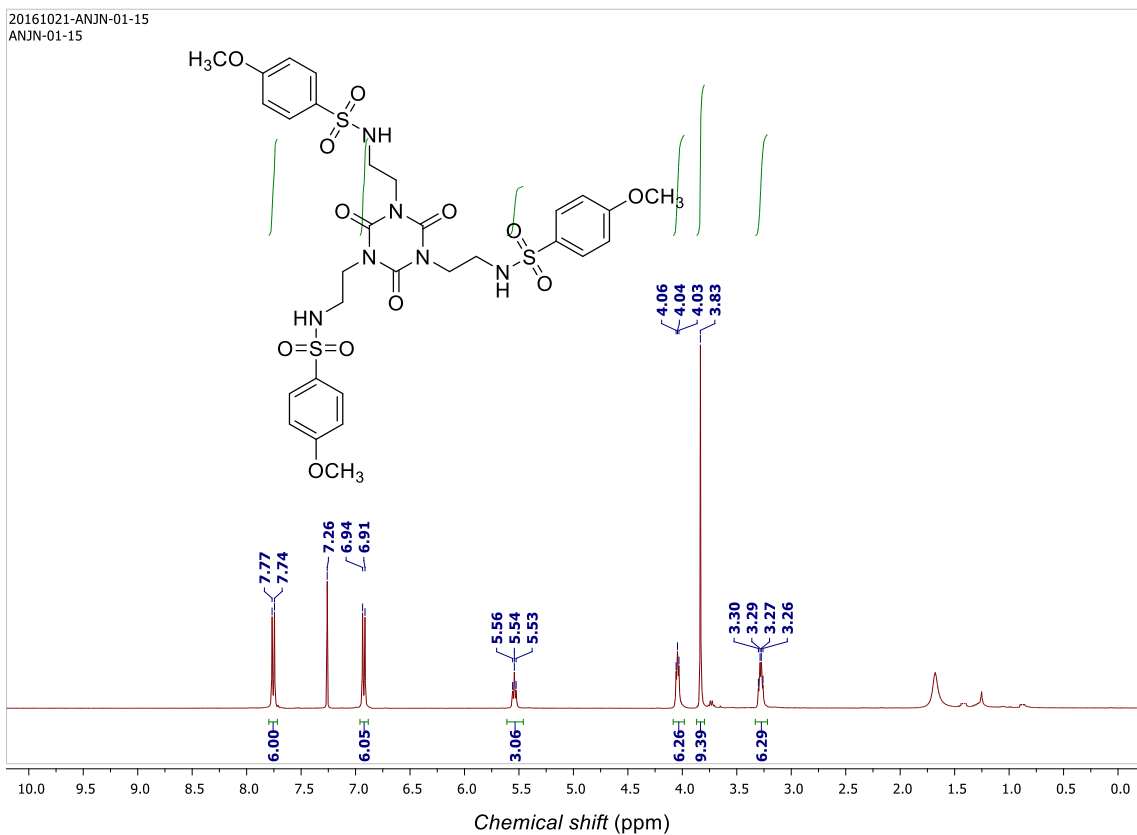


Fig. S44 ^1H NMR spectrum of compound **2b** in CDCl_3 .

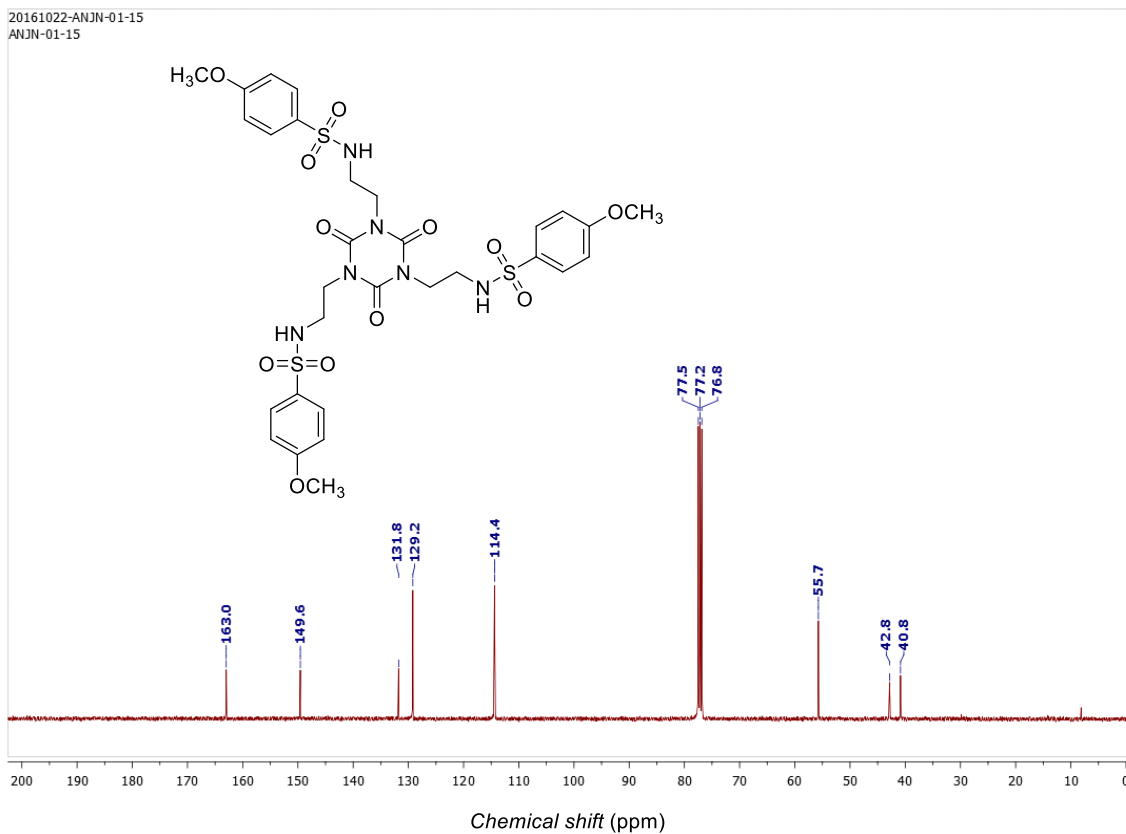


Fig. S45 ^{13}C NMR spectrum of compound **2b** in CDCl_3 .

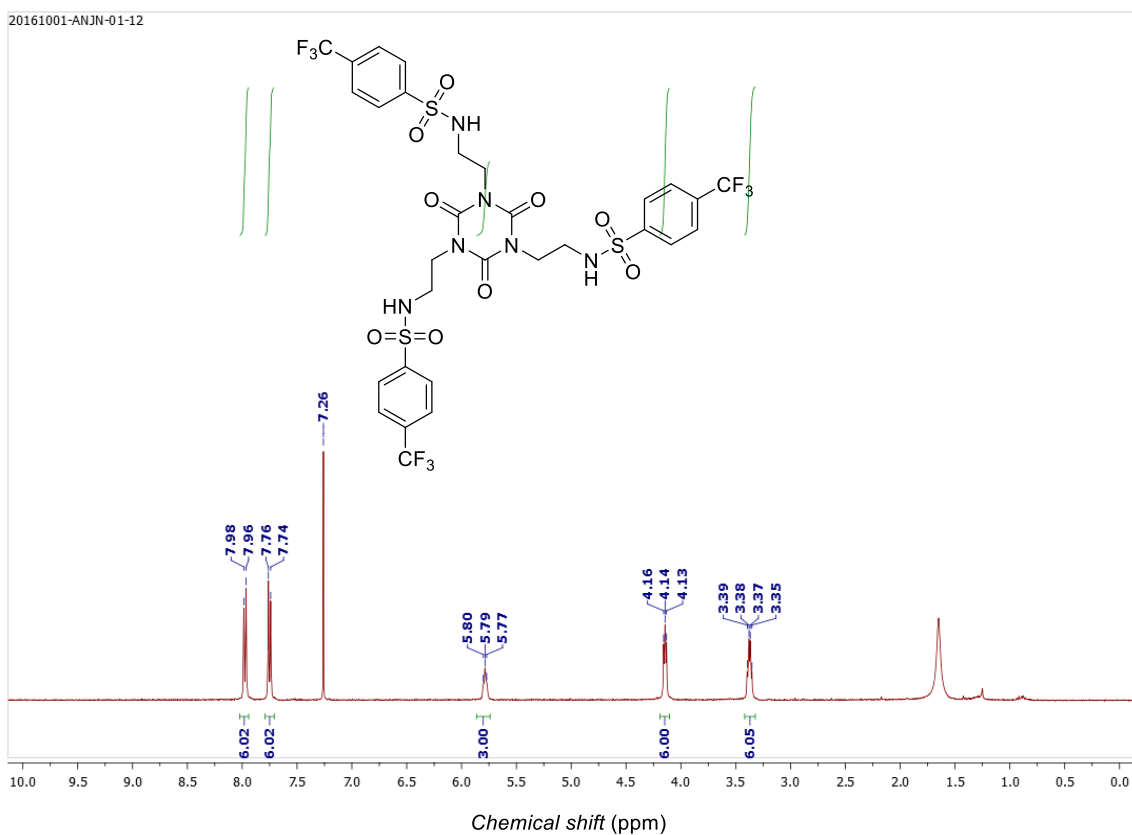


Fig. S46 ^1H NMR spectrum of compound **2c** in CDCl_3 .

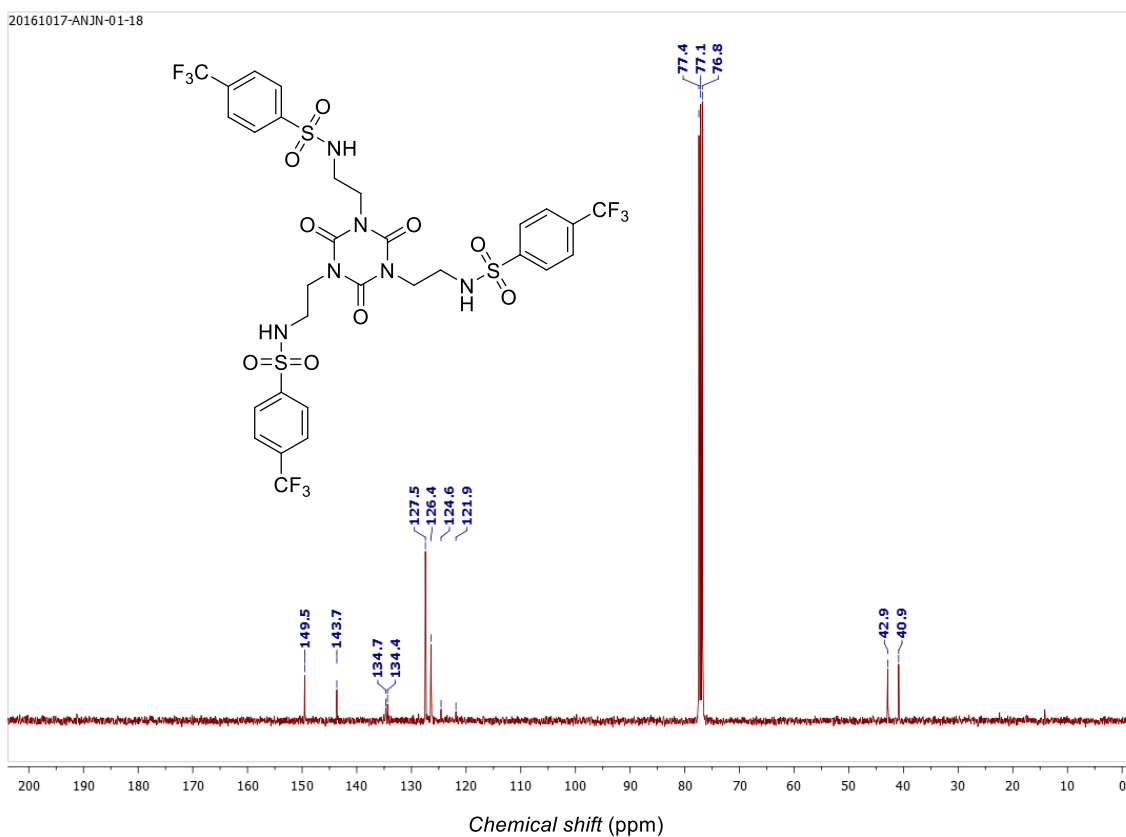


Fig. S47 ^{13}C NMR spectrum of compound **2c** in CDCl_3 .

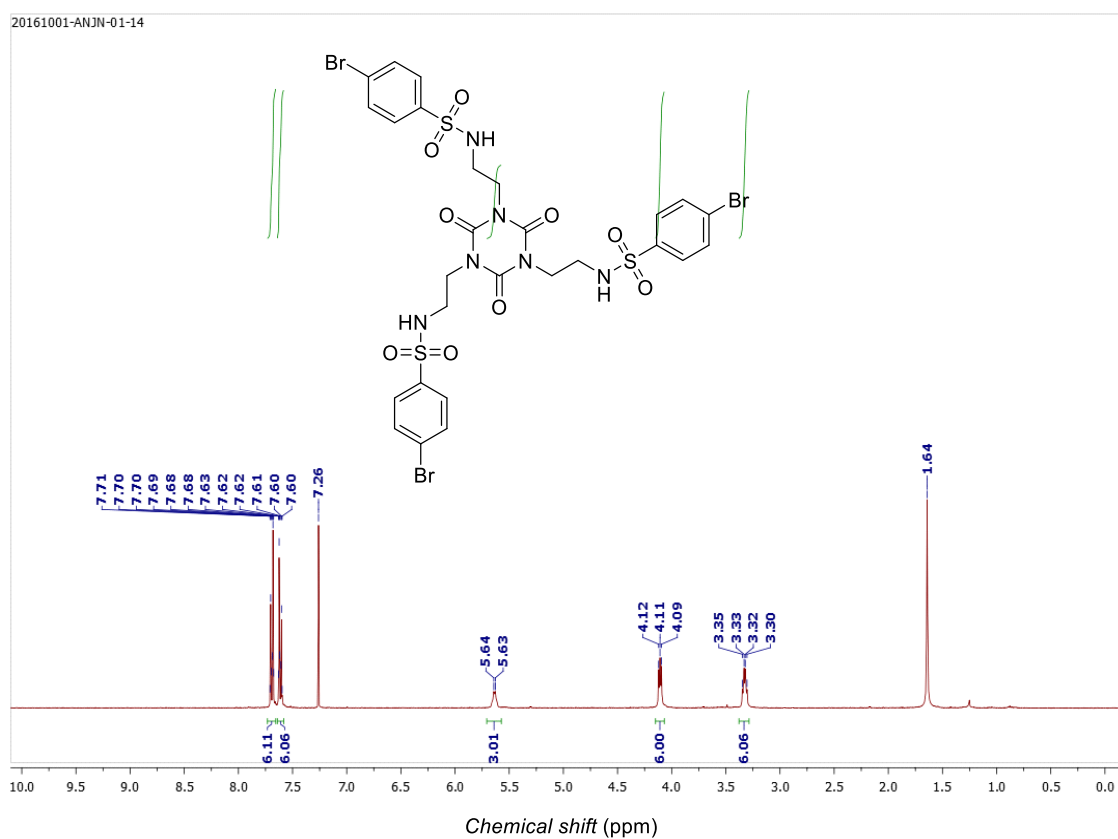


Fig. S48 ^1H NMR spectrum of compound **2d** in CDCl_3 .

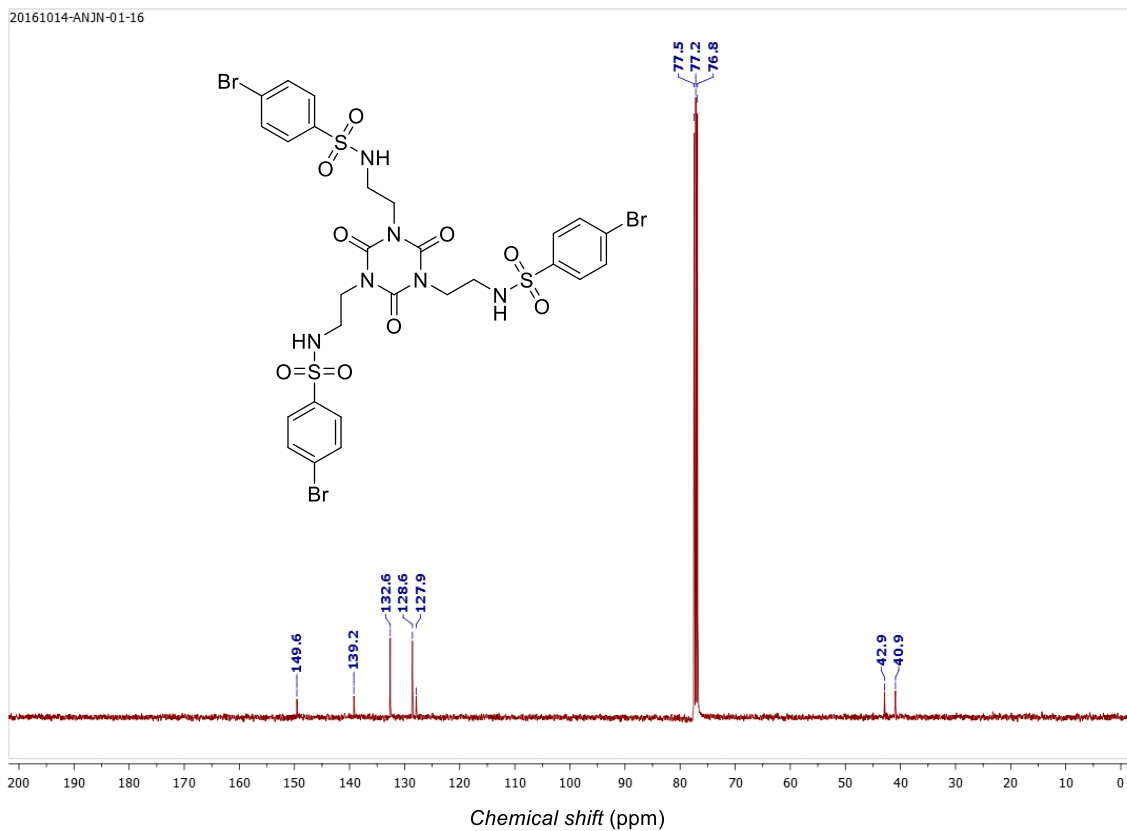


Fig. S49 ^{13}C NMR spectrum of compound **2d** in CDCl_3 .

8. References

- S1. I. Ravikumar, and P. Ghosh, *Chem. Commun.*, 2010, **46**, 6741-6743.
- S2. F. Hettche and R. W. Hoffmann, *New J. Chem.*, 2003, **27**, 172-177.
- S3. M. Wenzel, M. E. Light, A. P. Davis and P. A. Gale, *Chem. Commun.*, 2011, **47**, 7641-7643.
- S4. P. Thordarson, *Chem. Soc. Rev.*, 2011, **40**, 1305-1323.
- S5. H. Goto, E. Osawa, *J. Am. Chem. Soc.* **1989**, *111*, 8950-8951.
- S6. H. Goto, S. Obata, N. Nakayama and K. Ohta, CONFLEX 8, CONFLEX Corporation, Tokyo, Japan, 2017.
- S7. M. J. Frisch, G. W. Trucks, H. B. Schlegel, G. E. Scuseria, M. A. Robb, J. R. Cheeseman, G. Scalmani, V. Barone, B. Mennucci, G. A. Petersson, H. Nakatsuji, M. Caricato, X. Li, H. P. Hratchian, A. F. Izmaylov, J. Bloino, G. Zheng, J. L. Sonnenberg, M. Hada, M. Ehara, K. Toyota, R. Fukuda, J. Hasegawa, M. Ishida, T. Nakajima, Y. Honda, O. Kitao, H. Nakai, T. Vreven, J. A. Montgomery Jr., J. E. Peralta, F. Ogliaro, M. J. Bearpark, J. Heyd, E. N. Brothers, K. N. Kudin, V. N. Staroverov, R. Kobayashi, J. Normand, K. Raghavachari, A. P. Rendell, J. C. Burant, S. S. Iyengar, J. Tomasi, M. Cossi, N. Rega, N. J. Millam, M. Klene, J. E. Knox, J. B. Cross, V. Bakken, C. Adamo, J. Jaramillo, R. Gomperts, R. E. Stratmann, O. Yazyev, A. J. Austin, R. Cammi, C. Pomelli, J. W. Ochterski, R. L. Martin, K. Morokuma, V. G. Zakrzewski, G. A. Voth, P. Salvador, J. J. Dannenberg, S. Dapprich, A. D. Daniels, Ö. Farkas, J. B. Foresman, J. V. Ortiz, J. Cioslowski, D. J. Fox, Gaussian, Inc., Wallingford, CT, USA, 2009.
- S8. M. J. Frisch, J. A. Pople and J. S. Binkley, *J. Chem. Phys.*, 1984, **80**, 3265-3269.
- S9. S. F. Boys and F. Bernardi, *Mol. Phys.*, 1970, **19**, 553-566.
- S10. K. Kano and J. H. Fendler, *Biochim. Biophys. Acta, Biomembr.*, 1978, **509**, 289-299.